This article has been accepted for publication in a future issue of this journal, but has not been fully edited. Content may change prior to final publication. Citation information: DOI 10.1109/TCOMM.2017.2654448, IEEE Transactions on Communications

Modeling and performance analysis of wireless networks with ambient backscatter devices

Donatella Darsena, *Senior Member, IEEE,* Giacinto Gelli, and Francesco Verde, *Senior Member, IEEE*

***Abstract*—Ambient backscatter is an intriguing wireless communication paradigm that allows small devices to compute and communicate by using only the power they harvest from far-field radio-frequency (RF) signals in the air. Ambient backscattering devices reflect RF signals emitted by existing or legacy communications systems, such as digital TV broadcasting, cellular or Wi-Fi ones, which are designed for transporting information and are not intended for RF energy transfer. This paper deals with mathematical modeling and performance analysis of wireless broadband networks operating over fading channels with ambient backscatter devices. After introducing a detailed signal model of the relevant communication links, we study the influence of physical parameters on the capacity of both legacy and backscatter channels, by considering different receiver architectures. We analytically show that, under reasonable operative conditions, a legacy system – employing an orthogonal frequency-division multiplexing (OFDM) modulation scheme – can turn the RF interference arising from the backscatter process into a form of multipath diversity that can be exploited to increase its performance. Moreover, our analysis proves that a backscatter system – transmitting one symbol per OFDM symbol of the legacy system – can achieve satisfactory data rates over relatively short distances, especially when the intended recipient of the backscatter signal is co-located with the legacy transmitter, i.e., they are on the same device.**

***Index Terms*—Ambient backscatter, ergodic and outage capacity, symbol variance and amplitude constraints, multicarrier systems, performance bounds.**

I. Introduction

ELECTROMAGNETIC (EM) interference, also called radio-frequency (RF) interference, has been traditionally treated as a disturbance in the design of wireless communications systems. However, RF signals carry information as well as energy at the same time. Such a dual nature of EM interference has stimulated a great deal of interest for communications systems powered by harvested ambient energy. In particular, *ambient backscatter* has emerged as a novel communication paradigm, where a small passive device can transmit its own data by backscattering the EM far-field wave deriving from ambient RF transmitters. Such sources may be existing or *legacy* communication systems, such as digital TV (DTV) broadcasting, cellular systems, or wireless local area networks (LANs), e.g., Wi-Fi, which are mainly designed for transferring information and are not intended for RF energy transfer. Unlike traditional backscatter systems, such as radio frequency identification (RFID) ones [1], [2], ambient backscatter does not require a dedicated reader, which allows for direct device-to-device (D2D) [3] and even multi-hop communications. Recently, this new communication paradigm has been receiving much attention [4], [5], [6], [7], [8], [9], since it can be embedded into inexpensive objects in order to fulfil the ubiquitous and pervasive communication vision of the upcoming Internet-of-Things/Everything (IoT/IoE) concepts [3], [10]. Other applications of ambient backscatter are envisioned to include smart RFID tags with enhanced communication capabilities, large-scale commercial and industrial wireless sensor networks, as well as wireless body area network for health monitoring and medical applications [11], [12].

The main principles of ambient backscatter were first introduced in [4], where also a simple prototype is developed, which harvests DTV energy to achieve D2D communications with rates of 1 kbps over a range of about 8 m outdoor and 5 m indoor. In [5], the same principles are exploited to allow a passive device or *tag* to directly connect to the Internet by leveraging on an existing Wi-Fi infrastructure. In particular, in the scenario of [5], the tag can establish bidirectional communications with a Wi-Fi device by modulating the channel state information (CSI) or received signal strength indicator (RSSI) of the Wi-Fi channel (in the uplink) or by simple on-off modulation (in downlink), achieving rates of 0.5 kbps in uplink over a range of 1 m and up to 20 kbps over 2.2 m in downlink. A significant improvement over this scheme is the BackFi system proposed in [6], wherein backscatter communications can achieve at least 1 Mbps over a 5m-range in uplink, by exploiting the signal cancellation principles of full-duplex systems [13].

In [7], [8], [9] the ambient backscatter approach is extended to systems where the backscatter receiver (called the reader) is equipped with multiple antennas; moreover, a detailed analysis of the system from a signal processing perspective is carried out, by assuming that the wireless channel obeys a frequency-flat block-fading model. Since the tag employs low-rate differentially-encoded on-off signaling, the reader can decode its information by employing simple noncoherent detection strategies. The performance analysis of the approach proposed in [7], [8], [9] is carried out in terms of bit-error rate (BER), both analytically and by Monte Carlo simulations.

Existing research on ambient backscatter has covered both experimental and theoretical aspects. However, to the best

Manuscript received May 14, 2016; revised October 16, 2016 and January 12, 2017; accepted January 13, 2017. The associate editor coordinating the review of this paper and approving it for publication was Prof. M. Juntti.

D. Darsena is with the Department of Engineering, Parthenope University, Naples I-80143, Italy (e-mail: darsena@uniparthenope.it).

G. Gelli and F. Verde are both with the Department of Electrical Engineering and Information Technology, University Federico II, Naples I-80125, Italy [e-mail: (f.verde, gelli)@unina.it].

This article has been accepted for publication in a future issue of this journal, but has not been fully edited. Content may change prior to final publication. Citation information: DOI 10.1109/TCOMM.2017.2654448, IEEE Transactions on Communications

of our knowledge, an investigation of the ultimate performance limits of ambient backscatter, in terms of information-theoretic metrics, such as the ergodic or outage capacity, is still lacking. We aim at filling this gap, by evaluating in this paper the capacity (i.e., the maximum achievable transmission rate) of ambient backscatter communications systems.[1] Our analysis assumes that the legacy system employs an orthogonal frequency-division multiplexing (OFDM) scheme, which is ubiquitous in modern communication systems, whereas the backscatter system works at lower data-rates by transmitting a single symbol for each OFDM symbol of the legacy system. We evaluate typical information-theoretic figures of merit for both the legacy and the backscatter systems, by assuming a symbol variance constraint for the legacy system and both symbol variance and amplitude constraints for the backscatter one. Our results allow one to assess the maximum data-rate achievable by the backscatter system, and also show that, since the backscatter transmitter acts as a relay towards the legacy receiver, the legacy system can even benefit of ambient backscatter, provided that some reasonable assumptions are met. In other words, ambient backscatter is not only a viable means of opportunistically capitalizing on the energy carried out by RF signals, but it is also a way of turning EM interference into a form of diversity.

The paper is organized as follows. The system model and the general assumptions are introduced in Section II. The analytical performance analysis is carried out in Sections III and IV for the legacy and the backscatter system, respectively. Numerical results corroborating our analysis are reported in Section V. Conclusions are drawn in Section VI.

A. Notations

Besides standard notations, we adopt the following ones: matrices [vectors] are denoted with upper [lower] case bold-face letters (e.g., $\mathbf{A}$ or $\mathbf{a}$); the superscripts $*$, T, H, and -1 denote the conjugate, the transpose, the conjugate transpose (hermitian), and the inverse of a matrix, respectively; $\log(\cdot)$ is taken to the base 2; the operator $\mathbb{E}(\cdot)$ denotes ensemble averaging; $\mathbf{O}_{m\times n} \in \mathbb{R}^{m\times n}$ and $\mathbf{I}_m \in \mathbb{R}^{m\times m}$ denote the null and the identity matrices, respectively; matrix $\mathbf{A} = \mathrm{diag}(a_0, a_1, \ldots, a_{n-1})$ is diagonal; $\mathbf{F} \in \mathbb{R}^{n\times n}$ and $\mathbf{B} \in \mathbb{R}^{n\times n}$ denote the Toeplitz "forward shift" and "backward shift" matrices [15], respectively, where the first column of $\mathbf{F}$ and the first row of $\mathbf{B}$ are given by $[0, 1, 0, \ldots, 0]^T$ and $[0, 1, 0, \ldots, 0]$, respectively; a circular symmetric complex Gaussian random vector $\mathbf{x} \in \mathbb{C}^n$ with mean $\boldsymbol{\mu} \in \mathbb{C}^n$ and covariance matrix $\mathbf{K} \in \mathbb{C}^{n\times n}$ is denoted as $\mathbf{x} \sim \mathcal{CN}(\boldsymbol{\mu}, \mathbf{K})$.

II. Ambient backscatter system model

In this section, we introduce a model for ambient backscatter communications that harvest energy from legacy transmissions [4], [5], [6]. In particular, hereinafter, similarly to [4], the term *legacy* refers to existing wireless communications technologies, such as, e.g., DTV, cellular, and Wi-Fi systems.

[1]Preliminary results of this work were presented in [14].

The considered wireless network is composed of a legacy transmitter-receiver (LTx/LRx) pair and a *backscatter* transmitter (BTx) that wishes to transmit information-bearing symbols to an intended recipient (BRx). The devices LTx, BTx, LRx, and BRx will be also labelled as nodes 1, 2, 3, and 4, respectively. Specifically, the LTx and LRx are *active* devices, i.e., they have internal power sources to modulate and demodulate, respectively, the relevant RF signals. On the other hand, the BTx is a *passive* device, i.e., it does not include any active RF component, and communicates using only the power that it harvests from the RF signals transmitted by the LTx. The BRx may be either passive or might use typical active RF electronics to demodulate the signal backscattered by the BTx. In this respect, as depicted in Fig. 1, we consider two different network configurations: in the former one (left-side plot), the BRx and the LTx are co-located on the same device [5], [6], denoted as the legacy transceiver (LTRx); in the latter one (right-side plot), the BRx and the LTx are spatially-separated nodes [4]. The difference between such scenarios is mathematically relevant only when the signal model at the BRx (see Subsection II-C) and performance analysis of the backscatter system (see Section IV) are of concern.

The LTx adopts a conventional OFDM scheme with M subcarriers. The block of data to be transmitted by the LTx within the nth ($n \in \mathbb{Z}$) symbol of length T_s is denoted as $\mathbf{s}(n) \triangleq [s^{(0)}(n), s^{(1)}(n), \ldots, s^{(M-1)}(n)]^\mathrm{T} \in \mathbb{C}^M$, whose entries are independent and identically distributed (i.i.d.) zero-mean circularly symmetric complex symbols, with variance $\sigma_s^2 \triangleq \mathbb{E}[|s^{(m)}(n)|^2]$, for any $m \in \mathcal{M} \triangleq \{0, 1, \ldots, M-1\}$ and $n \in \mathbb{Z}$. The vector $\mathbf{s}(n)$ is subject to conventional OFDM precoding, encompassing M-point inverse discrete Fourier transform (IDFT), followed by cyclic prefix (CP) insertion of length $L_\mathrm{cp} < M$. It results that $T_\mathrm{s} \triangleq P\,T_\mathrm{c}$, with $P \triangleq M + L_\mathrm{cp}$ and T_c denoting the sampling period of the legacy system. The data block transmitted by the LTx can be compactly expressed [16] as $\mathbf{u}(n) = \mathbf{T}_\mathrm{cp}\,\mathbf{W}_\mathrm{IDFT}\,\mathbf{s}(n)$, where $\mathbf{T}_\mathrm{cp} \triangleq [\mathbf{I}_\mathrm{cp}^\mathrm{T}, \mathbf{I}_M]^\mathrm{T} \in \mathbb{R}^{P\times M}$, with $\mathbf{I}_\mathrm{cp} \in \mathbb{R}^{L_\mathrm{cp}\times M}$ obtained from $\mathbf{I}_M$ by picking its last L_cp rows, and $\mathbf{W}_\mathrm{IDFT} \in \mathbb{C}^{M\times M}$ is the unitary symmetric IDFT matrix [16]. The entries of $\mathbf{u}(n)$ are subject to D/A followed by RF conversion before being transmitted over the wireless channel.

On the other hand, due to its power limitation, the BTx transmits at a lower data-rate with respect to the legacy system – higher data-rates consume more power and energy. Specifically, the BTx has a Q-order symbol sequence $\{b(n)\}_{n\in\mathbb{Z}} \in \mathcal{B} \triangleq \{\beta_1, \beta_2, \ldots, \beta_Q\}$ of i.i.d. zero-mean circularly symmetric complex symbols to be transmitted toward the BRx, with variance $\sigma_b^2 \triangleq \mathbb{E}[|b(n)|^2]$, for any $n \in \mathbb{Z}$. The signaling interval of the backscatter system is equal to T_s, i.e., the BTx transmits only one of its symbols for each OFDM symbol of the legacy system. The sequence $\{b(n)\}_{n\in\mathbb{Z}}$ is arranged in consecutive frames of $B \in \mathbb{N}$ symbols, whose duration $T_\mathrm{f} \triangleq B\,T_s$ is less than or equal to the coherence time of the underlying channels.

A. Signal backscattered by the BTx

Since the BTx is passive, it cannot initiate transmissions on its own. Once the LTx transmits the block $\mathbf{u}(n)$, the EM wave

This article has been accepted for publication in a future issue of this journal, but has not been fully edited. Content may change prior to final publication. Citation information: DOI 10.1109/TCOMM.2017.2654448, IEEE Transactions on Communications

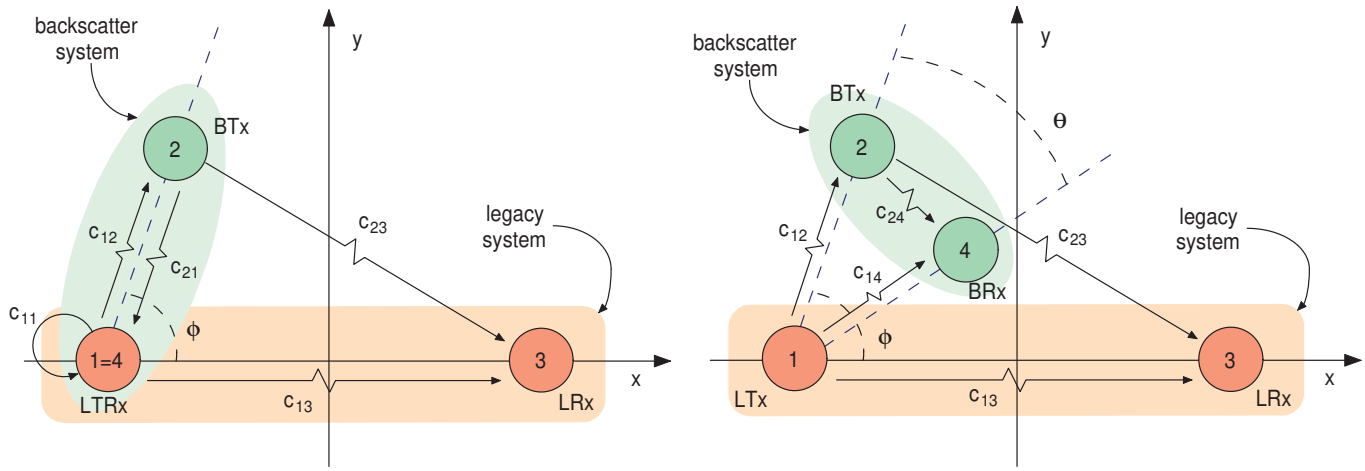

Figure 1. The considered wireless network model: nodes 1 and 3 represent the legacy transmitting and receiving devices; nodes 2 and 4 represent the backscatter transmitter and its intended recipient. We consider two different network configurations: in the left-side plot, nodes 1 and 4 are co-located on the same device; in the right-side plot, 1 and 4 are spatially-separated nodes.

propagates toward the BTx. When the wave reaches the BTx, its antenna is excited and the RF power is converted to direct current (DC) power through a *power harvester*. Once the BTx harvests enough RF power from the legacy signal, it will be activated. The harvested DC voltage is used to modulate the reflected EM wave and to power the digital logic units on the chip.

Regarding the $1 \to 2$ link, a frequency-selective and quasi-static channel model is assumed. Specifically, during a frame interval $T_{\rm f}$, the channel impulse response spans $L_{12} \triangleq \lceil \tau_{12}/T_{\rm c} \rceil$ sampling periods, with $\tau_{ik} \in \mathbb{R}$ denoting the maximum excess delay [17] of the $i \to k$ link. Hence, the resulting discrete-time channel $c_{12}(\ell)$ is a causal system of order L_{12}, i.e., $c_{12}(\ell) \equiv 0$ for $\ell \notin \{0, 1, \ldots, L_{12}\}$. Moreover, the $1 \to 2$ link is characterized by the (integer) time offset (TO) $\theta_{12} \triangleq \mathrm{int}(t_{12}/T_{\rm c})$ expressed in sampling periods, with $t_{ik} \in \mathbb{R}$ denoting the timing error (including propagation delay and time asynchronism between the transmitter and the receiver) of the $i \to k$ link.[2] Finally, since the BTx simply remodulates the carrier of the LTx, we assume in the sequel that the carrier frequency offset (CFO) is negligible.[3] The transmission of $\mathbf{u}(n)$ through the time-dispersive channel [18] between the LTx and the BTx introduces interblock interference (IBI) among successive blocks. The baseband-equivalent block received by the BTx within the nth OFDM symbol can be written as

$$\widetilde{\mathbf{r}}_2(n) = \widetilde{\mathbf{C}}_{12}^{(0)}\, \mathbf{u}(n) + \widetilde{\mathbf{C}}_{12}^{(1)}\, \mathbf{u}(n-1) \tag{1}$$

provided that $L_{12} + \theta_{12} \leq P - 1$,[4] where we have defined $\widetilde{\mathbf{r}}_2(n) \triangleq [r_2^{(0)}(n), r_2^{(1)}(n), \ldots, r_2^{(P-1)}(n)]^{\rm T} \in \mathbb{C}^P$, whereas

$$\widetilde{\mathbf{C}}_{12}^{(0)} \triangleq \sum_{\ell=0}^{L_{12}} c_{12}(\ell)\, \mathbf{F}^{\ell+\theta_{12}} \in \mathbb{C}^{P\times P} \tag{2}$$

$$\widetilde{\mathbf{C}}_{12}^{(1)} \triangleq \sum_{\ell=0}^{L_{12}} c_{12}(\ell)\, \mathbf{B}^{P-\ell-\theta_{12}} \in \mathbb{C}^{P\times P} \tag{3}$$

are Toeplitz lower- and upper-triangular matrices, respectively, and we have neglected the noise introduced by the BTx [1], [19], since the latter employs only passive components. It is worth noticing that the last $P - L_{12} - \theta_{12}$ rows of the matrix $\widetilde{\mathbf{C}}_{12}^{(1)}$ are identically zero, that is, the IBI contribution is entirely contained in the first $L_{12} + \theta_{12}$ entries of $\widetilde{\mathbf{r}}_2(n)$.

In our ambient backscatter framework, the BTx acts as a digital multilevel modulator, mapping each information symbol onto a set of Q waveforms by means of a proper variation of its chip impedance [20]. In its simplest implementation, Fig. 2 reports the equivalent Thévenin circuit [21] of the BTx front-end, where the sine-wave generator V_0 models the sinusoidal voltage induced by the power density of the incident EM field, $Z^{\rm a} = R^{\rm a} + j\, X^{\rm a} \in \mathbb{C}$ is the antenna impedance, and $Z_q^{\rm c} = R_q^{\rm c} + j\, X_q^{\rm c} \in \mathbb{C}$ are Q distinct values of the BTx chip impedance, for $q \in \mathcal{Q} \triangleq \{1, 2, \ldots, Q\}$.[5] The maximum power available from the generator is given by $\mathcal{P}_{\rm max}^{\rm c} \triangleq |V_0|^2/(8\, R^{\rm a})$.

At the reference plane denoted by the dashed line in Fig. 2, due to the impedance discontinuity, two power waves are generated: a *(nonreflecting) forward wave* propagating to the right and a *(reflecting) backward wave* giving rise to the backscattered field. When the switch S_q is closed, i.e., the chip impedance of the BTx takes on the value $Z_q^{\rm c}$, the average power harvested by the BTx is given [22] by $\mathcal{P}_q^{\rm c} = (1 - |\Gamma_q|^2)\, \mathcal{P}_{\rm max}^{\rm c}$ $(q \in \mathcal{Q})$, where

$$\Gamma_q = \frac{(Z^{\rm a})^* - Z_q^{\rm c}}{Z^{\rm a} + Z_q^{\rm c}} \tag{4}$$

[2]The fractional TO is incorporated as part of $\{c_{12}(\ell)\}_{\ell=0}^{L_{12}}$.

[3]A CFO may occur as a result of the Doppler effect from a mobile BTx, which is unlikely to happen in static backscatter systems [4], [5], [6].

[4]In general, the received block within the nth OFDM symbol is affected not only by the IBI of the previous $(n-1)$th symbol, but also by that of the $(n-2)$th one. Hereinafter, the assumption $L_{ik} + \theta_{ik} \leq P - 1$ ensures that, with reference to the generic $i \to k$ link, the sum of the TO and the channel order turns out to be within one OFDM symbol, such that the nth received block is impaired only by the IBI of the previous symbol.

[5]Other implementations of a backscatter modulator are possible, e.g., by using a digital-to-analog converter to drive the variable impedance [23].

This article has been accepted for publication in a future issue of this journal, but has not been fully edited. Content may change prior to final publication. Citation information: DOI 10.1109/TCOMM.2017.2654448, IEEE Transactions on Communications

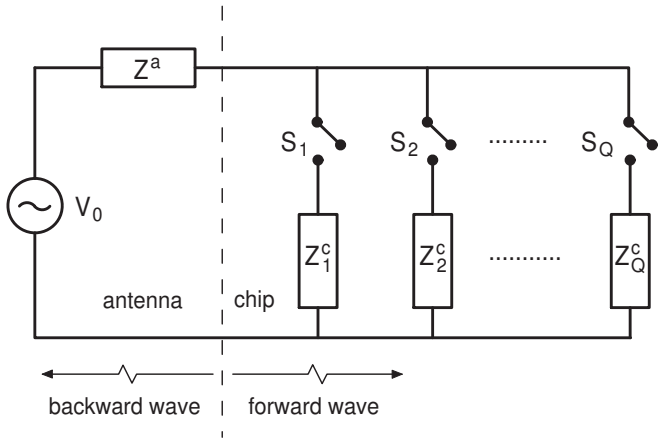

Figure 2. Equivalent Thévenin circuit of a simple implementation of a multilevel backscatter transmitter.

is the *power wave reflection coefficient* $\Gamma_q \in \mathbb{C}$, which is assumed to be constant.[6] The squared magnitude of the power wave reflection coefficient $0 \leq |\Gamma_q|^2 \leq 1$ is referred to as the *power reflection coefficient* [22]: it measures the fraction of $\mathcal{P}^{\mathrm{c}}_{\max}$ that is not delivered to the chip of the BTx. We note that, if $(Z^{\mathrm{a}})^* = Z^{\mathrm{c}}_q$ (*impedance matching condition*), then $\Gamma_q = 0$: in this case, the BTx harvests the maximum power $\mathcal{P}^{\mathrm{c}}_{\max}$ and, in theory, there is no backscattered field. Hence, an impedance mismatch $(Z^{\mathrm{a}})^* \neq Z^{\mathrm{c}}_q$ at the BTx is necessary to reflect part of the energy back to the intended recipient BRx.

The symbol sequence $\{b(n)\}_{n\in\mathbb{Z}}$ can be mapped to the backscattered signal by carefully choosing the chip impedances $Z^{\mathrm{c}}_1, Z^{\mathrm{c}}_2, \ldots, Z^{\mathrm{c}}_Q$. Each chip impedance in Fig. 2 corresponds to a point of the symbol constellation $\mathcal{B}$. More precisely, to produce impedance values realizable with passive components, all the power wave reflection coefficients $\Gamma_1, \Gamma_2, \ldots, \Gamma_Q$ are confined in the complex plane within a circle centered at the origin with radius smaller than or equal to one. These coefficients are then scaled by a constant $0 \leq \alpha \leq 1$ such that

$$\Gamma_q = \alpha\, \beta_q \quad (q \in \mathcal{Q}) \tag{5}$$

with $|\beta_q| \leq 1$. Eq. (5) establishes a one-to-one mapping between the information symbols of the BTx and the power wave reflection coefficients of its chip. Such a mapping is generally referred to as *backscatter* or *load modulation* [20]. The choice of α governs the harvesting-performance tradeoff of the backscatter communication process. Indeed, values of α closer to one allow the BTx to reflect increasing amounts of the incident field back to the BRx, resulting thus in greater backscatter signal strengths (i.e., for a target symbol error probability at the BRx, larger communication ranges). On the other hand, values of α much smaller than one allow a larger part of the incident field to be absorbed by the RF-to-DC conversion circuits of the BTx, hence improving power conversion (i.e., $\mathcal{P}^{\mathrm{c}}_q$) at the expense of backscatter signal strength. We note that $\alpha = 0$ accounts for the case when the backscatter system is in sleep mode and, hence, only the legacy transmission is active.

Once α and $\mathcal{B}$ have been chosen and, thus, the power wave reflection coefficients are identified through (5), the chip impedances $Z^{\mathrm{c}}_1, Z^{\mathrm{c}}_2, \ldots, Z^{\mathrm{c}}_Q$ corresponding to the designed signal constellation can be obtained from (4) as follows

$$Z^{\mathrm{c}}_q = \frac{(Z^{\mathrm{a}})^* - Z^{\mathrm{a}}\,\Gamma_q}{1 + \Gamma_q} \quad (q \in \mathcal{Q}) \tag{6}$$

where Z^{a} is a given parameter. In practice, some constraints may be imposed on the chip impedances (6): for instance, to use high-quality electronic components and/or reduce the physical size of the BTx, it might be required to use resistors and capacitors, by hence eliminating inductors [20]. For instance, let us assume that the BTx employs a QPSK constellation, i.e., there are $Q = 4$ symbols $\beta_1 = \exp(j\theta_1)$, $\beta_2 = \exp(j\theta_2)$, $\beta_3 = \exp(j\theta_3)$, and $\beta_4 = \exp(j\theta_4)$ in the constellation set $\mathcal{B}$ separated by $90°$. In this case, the BTx picks out two bits at a time from its own information-bearing bit sequence, maps them to the appropriate QPSK symbol $\beta_{\overline{q}}$, with $\overline{q} \in \{1, 2, 3, 4\}$, and, then, multiplies the signal received from the LTx by $\alpha\, \exp(j\theta_{\overline{q}})$ throughout an OFDM symbol. Such a multiplication is obtained by keeping closed the switch $S_{\overline{q}}$ for an OFDM symbol interval and choosing $Z^{\mathrm{c}}_{\overline{q}} = [(Z^{\mathrm{a}})^* - Z^{\mathrm{a}}\,\alpha\, \exp(j\theta_{\overline{q}})\,]/[1 + \alpha\, \exp(j\theta_{\overline{q}})]$.

According to the antenna scatterer theorem [26], the EM field backscattered from the antenna of the BTx can be divided into load-dependent (or *antenna mode*) scattering and load-independent (or *structural mode*) one: the former component can be associated with re-radiated power and depends on the chip impedances of the BTx, whereas the latter one can be interpreted as scattering from an open-circuited antenna. Therefore, with reference to antenna mode scattering and accounting for (5), the pth baseband-equivalent T_c-spaced sample backscattered by the BTx during the nth OFDM symbol of the legacy system assumes the expression $x_2^{(p)}(n) = \Gamma(n)\, r_2^{(p)}(n)$ $(p \in \mathcal{P})$, where $\Gamma(n) \triangleq \alpha\, b(n)$ is a discrete random variable assuming the values $\Gamma_1, \Gamma_2, \ldots, \Gamma_Q$, whereas $b(n) \in \mathcal{B}$ is the symbol transmitted by the BTx during the nth OFDM symbol. The corresponding block model reads as

$$\widetilde{\mathbf{x}}_2(n) = \Gamma(n)\, \widetilde{\mathbf{r}}_2(n) = \alpha\, b(n)\, \widetilde{\mathbf{r}}_2(n) \tag{7}$$

where $\widetilde{\mathbf{x}}_2(n) \triangleq [x_2^{(0)}(n), x_2^{(1)}(n), \ldots, x_2^{(P-1)}(n)]^{\mathrm{T}} \in \mathbb{C}^P$ and $\widetilde{\mathbf{r}}_2(n)$ is given by (1).

B. Signal received by the LRx

With reference to the $1 \to 3$ and $2 \to 3$ links, we maintain the same assumptions previously made for the $1 \to 2$ link: for $i \in \{1, 2\}$, within the time interval T_{f}, the resulting discrete-time channel $c_{i3}(\ell)$ is a causal system of order $L_{i3} \triangleq \lceil \tau_{i3}/T_{\mathrm{c}} \rceil$, i.e., $c_{i3}(\ell) \equiv 0$ for $\ell \notin \{0, 1, \ldots, L_{i3}\}$, and $\theta_{i3} \triangleq \mathrm{int}(t_{i3}/T_{\mathrm{c}})$ is the corresponding TO. Since the BTx reflects the RF signal transmitted by the LTx, both $1 \to 3$ and $2 \to 3$ transmissions occur at the same RF frequency. For such a reason, we assume that the corresponding CFOs are equal and is estimated and compensated at the LRx through conventional techniques [27].

[6]The power wave reflection coefficient Γ_q depends on the chip impedance which, in its turn, depends on the chip input power. A linearized model is assumed for the power wave reflection coefficient [24], according to which Γ_q does not depend on the incident power. Moreover, we neglect frequency variations of Γ_q, whose impact on system performance is negligible [25].

This article has been accepted for publication in a future issue of this journal, but has not been fully edited. Content may change prior to final publication. Citation information: DOI 10.1109/TCOMM.2017.2654448, IEEE Transactions on Communications

Provided that $L_{13}+\theta_{13}\leq P-1$ and $L_{23}+\theta_{23}\leq P-1$ (see footnote 4), accounting for (1) and (7), after CFO compensation, the baseband-equivalent vector received by the LRx within the nth OFDM symbol of the legacy system can be expressed as shown at the top of the next page in (8), where $\{\widetilde{\mathbf{C}}_{13}^{(0)},\widetilde{\mathbf{C}}_{13}^{(1)}\}$ and $\{\widetilde{\mathbf{C}}_{23}^{(0)},\widetilde{\mathbf{C}}_{23}^{(1)}\}$ can be obtained from (2) and (3) by replacing $\{L_{12},c_{12}(\ell),\theta_{12}\}$ with $\{L_{13},c_{13}(\ell),\theta_{13}\}$ and $\{L_{23},c_{23}(\ell),\theta_{23}\}$, respectively, and $\widetilde{\mathbf{v}}_3(n)\in\mathbb{C}^P$ accounts for the structural mode scattering, which is independent of the BTx chip impedances, as well as for thermal noise. We have observed that $\widetilde{\mathbf{C}}_{23}^{(1)}\,\widetilde{\mathbf{C}}_{12}^{(1)}=\mathbf{O}_{P\times P}$, under the assumption that

$$L_{12}+L_{23}+\theta_{12}+\theta_{23}\leq P-1\,. \tag{9}$$

The set of lower (upper) triangular Toeplitz matrices in (8) possesses an eminent algebraic structure: indeed, such a set is an *algebra* [15]. In particular, the product of any lower (upper) triangular Toeplitz matrices is a lower (upper) triangular Toeplitz matrix, too. Indeed, it is directly verified that, if (9) holds, the product $\widetilde{\mathbf{C}}_{23}^{(0)}\,\widetilde{\mathbf{C}}_{12}^{(0)}$ is a lower-triangular Toeplitz matrix having as first column $[\mathbf{0}_{\theta_{12}+\theta_{23}}^{\mathrm{T}},\mathbf{c}_{123}^{\mathrm{T}}(n),\mathbf{0}_{P-L_{12}-L_{23}-\theta_{12}-\theta_{23}-1}^{\mathrm{T}}]^{\mathrm{T}}$, where the vector $\mathbf{c}_{123}\in\mathbb{C}^{L_{12}+L_{23}+1}$ collects the samples of the (linear) convolution between $\{c_{12}(\ell)\}_{\ell=0}^{L_{12}}$ and $\{c_{23}(\ell)\}_{\ell=0}^{L_{23}}$. Under the assumption that

$$L_{\mathrm{cp}}\geq\max(L_{13}+\theta_{13},L_{12}+L_{23}+\theta_{12}+\theta_{23}) \tag{10}$$

the IBI contribution in (8) is discarded by dropping the first L_{cp} components of $\widetilde{\mathbf{r}}_3(n)$, since it is verified by direct inspection that: (i) only the first $L_{12}+L_{23}+\theta_{12}+\theta_{23}$ rows of $\widetilde{\mathbf{C}}_{23}^{(0)}\,\widetilde{\mathbf{C}}_{12}^{(1)}$ are possibly nonzero; (ii) the last $P-L_{23}-\theta_{23}$ rows of the matrix $\widetilde{\mathbf{C}}_{23}^{(1)}$ are identically zero and, hence, the nonzero entries of $\widetilde{\mathbf{C}}_{23}^{(1)}\,\widetilde{\mathbf{C}}_{12}^{(0)}$ are located within its first $L_{23}+\theta_{23}$ rows; (iii) the last $P-L_{13}-\theta_{13}$ rows of $\widetilde{\mathbf{C}}_{13}^{(1)}$ are identically zero. Therefore, if (10) is fulfilled, after discarding the CP, performing M-point discrete Fourier transform (DFT), the resulting frequency-domain data block $\mathbf{r}_3(n)\in\mathbb{C}^M$ reads as

$$\mathbf{r}_3(n)=\mathbf{\Psi}_3(n)\,\mathbf{s}(n)+\mathbf{v}_3(n) \tag{11}$$

where $\mathbf{\Psi}_3(n)\triangleq\mathrm{diag}[\Psi_3(n,0),\Psi_3(n,1),\ldots,\Psi_3(n,M-1)]$, whose diagonal entries are given by

$$\Psi_3(n,m)\triangleq\Psi_{13}(m)+\alpha\,b(n)\,\Psi_{12}(m)\,\Psi_{23}(m) \tag{12}$$

for $m\in\mathcal{M}$, with

$$\Psi_{ik}(m)\triangleq e^{-j\frac{2\pi}{M}\theta_{ik}m}\sum_{\ell=0}^{L_{ik}}c_{ik}(\ell)\,e^{-j\frac{2\pi}{M}\ell m} \tag{13}$$

and $\mathbf{v}_3(n)\in\mathbb{C}^M$ is obtained from $\widetilde{\mathbf{v}}_3(n)$ by discarding its first L_{cp} entries and performing M-point DFT. The entries of $\mathbf{\Psi}_3(n)$ can be estimated at the LRx using training symbols sent from the LTx, by completely ignoring that such channel parameters incorporate the backscattering effects.

Remark 1: It results from (11) and (12) that, due to the dependence of $\Psi_3(n,m)$ on the symbol $b(n)$ transmitted by the BTx, the LRx sees a *time-varying frequency-flat fading* channel for each subcarrier, which however remains constant over an OFDM symbol. Multicarrier systems operating over wireless channels are typically designed to perform symbol-by-symbol channel estimation and detection at the receiver. In this case, such a symbol-level time-variability of the legacy channel is irrelevant.

Remark 2: It is noteworthy from (8)-(11) that the signal backscattered by the BTx may create additional paths from the LTx to the LRx, which increases multipath propagation on the legacy channel. In particular, if $L_{12}+L_{23}+\theta_{12}+\theta_{23}>L_{13}+\theta_{13}$, in accordance with (10), such an additional multipath requires a corresponding increase of the CP length in order to avoid both IBI and intercarrier interference (ICI) after CP removal, which may worsen the performance of the legacy system. In summary, the price to pay for allowing ambient backscatter is an oversizing of the CP length, thus leading to an inherent reduction of the transmission data rate of the legacy system. However, such a loss turns out to be negligible if the number M of subcarriers is significantly greater than L_{cp}. Most important, we show in Section III that, if the legacy system is designed to fulfil (10), it might *even* achieve a performance gain.

Remark 3: Inequality (10) poses an upper limit to the tolerable maximum excess delay of the involved channels and to the maximum distances among the LTx, the BTx, and the LRx. It requires only upper bounds (rather than the exact knowledge) on the channel orders and TOs. This is a reasonable assumption in the considered scenario. Indeed, in general, depending on the transmitted signal parameters (carrier frequency and bandwidth) and environment (indoor or outdoor), the maximum channel multipath spread is known. For legacy systems, particular synchronization policies are adopted to reduce the asynchronisms [28], thus confining the TOs to a small uncertainty interval with predictable support.

C. Signal received by the BRx

Let us first consider the scenario when the BRx and the LTx are spatially-separated nodes, as reported in the right-side plot of Fig. 1. Concerning the $1\to4$ and $2\to4$ links, we maintain the same assumptions previously made for the $1\to2$, $1\to3$, and $2\to3$ links: in summary, for $i\in\{1,2\}$, within the coherence time T_{f}, the resulting discrete-time channel $c_{i4}(\ell)$ is a causal system of order $L_{i4}\triangleq\lceil\tau_{i4}/T_{\mathrm{c}}\rceil$, i.e., $c_{i4}(\ell)\equiv0$ for $\ell\notin\{0,1,\ldots,L_{i4}\}$, and $\theta_{i4}\triangleq\mathrm{int}(t_{i4}/T_{\mathrm{c}})$ is the corresponding TO. Similarly to Subsection II-B, we assume that the $1\to4$ and $2\to4$ links have the same CFO, which will be denoted as $\nu\in(-1/2,1/2)$ in the sequel (it is normalized to the subcarrier spacing $1/T_c$).

Under the assumption that $L_{14}+\theta_{14}\leq P-1$ and $L_{24}+\theta_{24}\leq P-1$ (see footnote 4), the baseband-equivalent block received by the BRx within the nth OFDM symbol of the legacy system can be expressed as shown at the top of the next page in (14), where $\{\widetilde{\mathbf{C}}_{14}^{(0)},\widetilde{\mathbf{C}}_{14}^{(1)}\}$ and $\{\widetilde{\mathbf{C}}_{24}^{(0)},\widetilde{\mathbf{C}}_{24}^{(1)}\}$ can be obtained from (2) and (3) by replacing $\{L_{12},c_{12}(\ell),\theta_{12}\}$ with $\{L_{14},c_{14}(\ell),\theta_{14}\}$ and $\{L_{24},c_{24}(\ell),\theta_{24}\}$, respectively, we have defined the diagonal matrix $\mathbf{\Sigma}_\nu\triangleq\mathrm{diag}[1,e^{j\frac{2\pi}{M}\nu},\ldots,e^{j\frac{2\pi}{M}\nu(P-1)}]\in\mathbb{C}^{P\times P}$, and

This article has been accepted for publication in a future issue of this journal, but has not been fully edited. Content may change prior to final publication. Citation information: DOI 10.1109/TCOMM.2017.2654448, IEEE Transactions on Communications

$$\begin{aligned}\widetilde{\mathbf{r}}_3(n) &= \widetilde{\mathbf{C}}_{13}^{(0)}\,\mathbf{u}(n) + \widetilde{\mathbf{C}}_{13}^{(1)}\,\mathbf{u}(n-1) + \widetilde{\mathbf{C}}_{23}^{(0)}\,\widetilde{\mathbf{x}}_2(n) + \widetilde{\mathbf{C}}_{23}^{(1)}\,\widetilde{\mathbf{x}}_2(n-1) + \widetilde{\mathbf{v}}_3(n)\\ &= \left[\widetilde{\mathbf{C}}_{13}^{(0)} + \alpha\, b(n)\,\widetilde{\mathbf{C}}_{23}^{(0)}\,\widetilde{\mathbf{C}}_{12}^{(0)}\right]\mathbf{u}(n) + \left[\widetilde{\mathbf{C}}_{13}^{(1)} + \alpha\, b(n)\,\widetilde{\mathbf{C}}_{23}^{(0)}\,\widetilde{\mathbf{C}}_{12}^{(1)} + \alpha\, b(n-1)\,\widetilde{\mathbf{C}}_{23}^{(1)}\,\widetilde{\mathbf{C}}_{12}^{(0)}\right]\mathbf{u}(n-1) + \widetilde{\mathbf{v}}_3(n) \qquad (8)\end{aligned}$$

$$\begin{aligned}\widetilde{\mathbf{r}}_4(n) &= e^{j\frac{2\pi}{M}\nu n P}\,\mathbf{\Sigma}_\nu\left[\widetilde{\mathbf{C}}_{14}^{(0)}\,\mathbf{u}(n) + \widetilde{\mathbf{C}}_{14}^{(1)}\,\mathbf{u}(n-1) + \widetilde{\mathbf{C}}_{24}^{(0)}\,\widetilde{\mathbf{x}}_2(n) + \widetilde{\mathbf{C}}_{24}^{(1)}\,\widetilde{\mathbf{x}}_2(n-1)\right] + \widetilde{\mathbf{v}}_4(n)\\ &= \alpha\, e^{j\frac{2\pi}{M}\nu n P}\,\mathbf{\Sigma}_\nu\left[\widetilde{\mathbf{C}}_{24}^{(0)}\,\widetilde{\mathbf{C}}_{12}^{(0)}\,\mathbf{u}(n) + \widetilde{\mathbf{C}}_{24}^{(0)}\,\widetilde{\mathbf{C}}_{12}^{(1)}\,\mathbf{u}(n-1)\right] b(n) + \alpha\, e^{j\frac{2\pi}{M}\nu n P}\,\mathbf{\Sigma}_\nu\,\widetilde{\mathbf{C}}_{24}^{(1)}\,\widetilde{\mathbf{C}}_{12}^{(0)}\,\mathbf{u}(n-1)\, b(n-1)\\ &\quad + e^{j\frac{2\pi}{M}\nu n P}\,\mathbf{\Sigma}_\nu\left[\widetilde{\mathbf{C}}_{14}^{(0)}\,\mathbf{u}(n) + \widetilde{\mathbf{C}}_{14}^{(1)}\,\mathbf{u}(n-1)\right] + \widetilde{\mathbf{v}}_4(n) \qquad (14)\end{aligned}$$

$\widetilde{\mathbf{v}}_4(n)\mathbb{C}^P$ accounts for both the structural mode scattering and thermal noise.

Remark 4: According to (14), the BRx experiences *frequency-selective fast fading*, since: (i) the received signal is corrupted by the intersymbol interference (ISI) of the previous symbol $b(n-1)$; (ii) the channel seen by the BRx varies with time from sampling period to sampling period, due to its dependence on the data $\{u^{(p)}(n)\}_{p=0}^{P-1}$ transmitted by the LTx, and such a variation is P-times faster than the symbol rate $1/T_s$ of the backscatter system.

Interestingly, by observing that the nonzero entries of $\mathbf{\Sigma}_\nu\,\widetilde{\mathbf{C}}_{24}^{(1)}\,\widetilde{\mathbf{C}}_{12}^{(0)}$ are located within its first $L_{24}+\theta_{24}$ rows and the last $P-L_{14}-\theta_{14}$ rows of $\mathbf{\Sigma}_\nu\,\widetilde{\mathbf{C}}_{14}^{(1)}$ are identically zero, the BRx can completely remove its own ISI and partially mitigate the interference generated by the legacy transmission through a simple removal of the first

$$L_b \geq \max\left(L_{14}+\theta_{14}, L_{24}+\theta_{24}\right) \qquad (15)$$

components of $\widetilde{\mathbf{r}}_4(n)$. This operation is accomplished by defining the matrix $\mathbf{R}_b \triangleq [\mathbf{O}_{N\times L_b}, \mathbf{I}_N] \in \mathbb{R}^{N\times P}$, with $N \triangleq P - L_b > 0$, and forming at the receiver the product $\mathbf{R}_b\,\widetilde{\mathbf{r}}_4(n)$. So doing, one has

$$\mathbf{R}_b\,\widetilde{\mathbf{r}}_4(n) = \alpha\,\mathbf{c}_4\, b(n) + \mathbf{d}_4(n) \qquad (16)$$

with

$$\mathbf{c}_4 \triangleq e^{j\frac{2\pi}{M}\nu n P}\,\mathbf{R}_b\,\mathbf{\Sigma}_\nu\left[\widetilde{\mathbf{C}}_{24}^{(0)}\,\widetilde{\mathbf{C}}_{12}^{(0)}\,\mathbf{u}(n) + \widetilde{\mathbf{C}}_{24}^{(0)}\,\widetilde{\mathbf{C}}_{12}^{(1)}\,\mathbf{u}(n-1)\right] \in \mathbb{C}^N \qquad (17)$$

$$\mathbf{d}_4(n) \triangleq e^{j\frac{2\pi}{M}\nu n P}\,\mathbf{R}_b\,\mathbf{\Sigma}_\nu\,\widetilde{\mathbf{C}}_{14}^{(0)}\,\mathbf{u}(n) + \mathbf{R}_b\,\widetilde{\mathbf{v}}_4(n) \in \mathbb{C}^N \qquad (18)$$

where it results that $\mathbf{R}_b\,\mathbf{\Sigma}_\nu\,\widetilde{\mathbf{C}}_{24}^{(1)}\,\widetilde{\mathbf{C}}_{12}^{(0)} = \mathbf{O}_{N\times P}$ and $\mathbf{R}_b\,\mathbf{\Sigma}_\nu\,\widetilde{\mathbf{C}}_{14}^{(1)} = \mathbf{O}_{N\times P}$. Similarly to (10) (see Remark 3), inequality (15) limits both the acceptable time-dispersion of the involved channels and the maximum distances among the LTx, BTx and BRx, and its fulfilment requires some *a priori* knowledge at the BRx.

When the intended recipient of the backscatter signal and the legacy transmitter are co-located on the same device (see the left-side plot of Fig. 1), namely, the LTRx, the reference signal model can be obtained from (16)–(18) by replacing the subscript 4 with 1 and setting $\nu = 0$, which implies that $\mathbf{\Sigma}_\nu = \mathbf{I}_P$. In this case, the matrix $\widetilde{\mathbf{C}}_{11}^{(0)}$ models a self-interference channel and $\widetilde{\mathbf{C}}_{11}^{(0)}\,\mathbf{u}(n)$ represents direct leakage between the LTx transmit/receive chains and/or reflections by other objects in the environment [6]. The key difference between such a scenario and conventional RFID backscatter [1] is that the signal transmitted by the LTx (i.e., the reader in RFID jargon) is an information-bearing multicarrier signal rather than an unmodulated carrier (i.e., a sinusoid). Hence, the self-interference cancellation and demodulation operations become significantly harder. In particular, as previously evidenced in Remark 4, the multicarrier signal emitted by the LTx gives rise to time variations of the channel seen by the BRx at a sampling-period scale.

D. General assumptions for the performance analysis

The goal of the forthcoming Sections III and IV is twofold. First, we aim at showing in Section III what is the influence of the backscatter communication on the achievable rates of the legacy system, by assuming that the CP is long enough, i.e., inequality (10) is fulfilled. Second, under assumption (15), we highlight in Section IV what are the ultimate rates of the backscatter communication, by considering either the case when the nodes BRx and LTx are co-located or the situation in which they are spatially-separated nodes. General assumptions for the analysis are reported in the sequel.

For $i \in \{1,2\}$ and $k \in \{2,3,4\}$, with $i \neq k$, the channel samples $c_{ik}(0), c_{ik}(1), \ldots, c_{ik}(L_{ik})$ (encompassing the physical channel as well as the transmit/receive filters) are modeled as i.i.d. zero-mean circularly symmetric complex Gaussian random coefficients (*Rayleigh fading model*),[7] which are constant within the coherence time T_{f}, but are allowed to vary independently in different coherence intervals; the variance $\mathbb{E}[|c_{ik}(\ell)|^2] \triangleq \sigma_{ik}^2/(L_{ik}+1)$ of the $i \to k$ link depends on the corresponding average path loss. Fading coefficients of different links are statistically independent

[7]Although the transmit/receive filters might introduce statistical correlation among channel taps, it is a common practice [28] to neglect such a correlation when evaluating the performance of multicarrier systems.

This article has been accepted for publication in a future issue of this journal, but has not been fully edited. Content may change prior to final publication. Citation information: DOI 10.1109/TCOMM.2017.2654448, IEEE Transactions on Communications

among themselves, i.e., $c_{i_1k_1}(\ell)$ is statistically independent of $c_{i_2k_2}(\ell)$ for $i_1 \neq i_2$ or $k_1 \neq k_2$. Since $c_{ik}(\ell)$ is a circularly symmetric complex Gaussian random variable by assumption, then $c_{ik}(\ell)$ and $c_{ik}(\ell)\, e^{-j\frac{2\pi}{M}(\ell+\theta_{ik})m}$ have the same probability distribution [29], i.e., $c_{ik}(\ell)\, e^{-j\frac{2\pi}{M}(\ell+\theta_{ik})m} \sim \mathcal{CN}[0, \sigma_{ik}^2/(L_{ik}+1)]$, for any ℓ, m, and n. Consequently, one has $\Psi_{ik}(m) \sim \mathcal{CN}(0, \sigma_{ik}^2)$. It is seen from (13) that, even if the time-domain channel taps $\{c_{ik}(\ell)\}_{\ell=0}^{L_{ik}}$ are assumed to be uncorrelated, the corresponding DFT samples $\Psi_{ik}(m_1)$ and $\Psi_{ik}(m_2)$ turn out to be correlated, for $m_1 \neq m_2 \in \mathcal{M}$. For $k \in \{3, 4\}$, we assume that $\widetilde{\mathbf{v}}_k(n) \sim \mathcal{CN}(\mathbf{0}_P, \sigma_{v_k}^2\, \mathbf{I}_P)$ with $\mathbb{E}[\widetilde{\mathbf{v}}_k(n_1)\, \widetilde{\mathbf{v}}_k^{\mathrm{H}}(n_2)] = \mathbf{O}_{P\times P}$, for $n_1 \neq n_2 \in \mathbb{Z}$.

Finally, channel coefficients, information-bearing symbols, and noise samples are all modeled as statistically independent random variables.

III. Capacity analysis of the legacy system

Since the detection process at the LRx is carried out on a symbol-by-symbol basis, we omit the dependence on the symbol index n hereinafter. Under the assumption that the realization $\mathbf{\Xi}_3$ of $\mathbf{\Psi}_3$ is known at the LRx (but not at the LTx), the channel output of (11) is the pair $(\mathbf{r}_3, \mathbf{\Psi}_3)$. Therefore, the *(coherent) ergodic (or Shannon) capacity* of (11) is defined as (see, e.g., [30])

$$\mathsf{C}_3 \triangleq \sup_{f(\mathbf{s})\in\mathcal{I}_s} \frac{\mathsf{I}(\mathbf{s}; \mathbf{r}_3, \mathbf{\Psi}_3)}{M} \quad \text{(in b/s/Hz)} \tag{19}$$

where $f(\mathbf{s})$ is the probability density function (pdf) of $\mathbf{s}$, $\mathcal{I}_s$ is the set of admissible input distributions having the variance constraint $\mathbb{E}(\|\mathbf{s}\|^2) = M\sigma_s^2$ and $\mathsf{I}(\mathbf{s}; \mathbf{r}_3, \mathbf{\Psi}_3)$ denotes the mutual information [31], [32] between $\mathbf{s}$ and $(\mathbf{r}_3, \mathbf{\Psi}_3)$. The ergodic capacity can be achieved if the length of the codebook is long enough to reflect the ergodic nature of fading [33] (i.e., the duration of each transmitted codeword is much greater than the channel coherence time).

By using the chain rule for mutual information [31], [32] and observing that $\mathbf{s}$ and $\mathbf{\Psi}_3$ are statistically independent, it results that $\mathsf{I}(\mathbf{s}; \mathbf{r}_3, \mathbf{\Psi}_3) = \mathsf{I}(\mathbf{s}; \mathbf{\Psi}_3) + \mathsf{I}(\mathbf{s}; \mathbf{r}_3 \,|\, \mathbf{\Psi}_3) = \mathsf{I}(\mathbf{s}; \mathbf{r}_3 \,|\, \mathbf{\Psi}_3) = \mathbb{E}_{\mathbf{\Psi}_3}[\mathsf{I}(\mathbf{s}; \mathbf{r}_3 \,|\, \mathbf{\Psi}_3 = \mathbf{\Xi}_3)]$, where $\mathsf{I}(\mathbf{s}; \mathbf{r}_3 \,|\, \mathbf{\Psi}_3)$ is the mutual information between $\mathbf{s}$ and $\mathbf{r}_3$, given $\mathbf{\Psi}_3$. It is shown in [30] that, given $\mathbf{\Psi}_3 = \mathbf{\Xi}_3$, the input distribution that maximizes $\mathsf{I}(\mathbf{s}; \mathbf{r}_3 \,|\, \mathbf{\Psi}_3 = \mathbf{\Xi}_3)$ is $\mathbf{s} \sim \mathcal{CN}(\mathbf{0}_M, \sigma_s^2\, \mathbf{I}_M)$ and the corresponding maximal mutual information $\mathsf{I}_{\max}(\mathbf{s}; \mathbf{r}_3 \,|\, \mathbf{\Psi}_3 = \mathbf{\Xi}_3)$ is given by

$$\mathsf{I}_{\max}(\mathbf{s}; \mathbf{r}_3 \,|\, \mathbf{\Psi}_3 = \mathbf{\Xi}_3) = \log\det\left(\mathbf{I}_M + \frac{\sigma_s^2}{\sigma_{v_3}^2}\, \mathbf{\Xi}_3\, \mathbf{\Xi}_3^{\mathrm{H}}\right) . \tag{20}$$

Consequently, one has

$$\begin{aligned}\mathsf{C}_3 &= \frac{1}{M}\, \mathbb{E}\left[\log\det\left(\mathbf{I}_M + \frac{\sigma_s^2}{\sigma_{v_3}^2}\, \mathbf{\Psi}_3\, \mathbf{\Psi}_3^{\mathrm{H}}\right)\right] \\ &= \frac{1}{M}\sum_{m=0}^{M-1} \mathbb{E}\left[\log\left(1 + \frac{\sigma_s^2}{\sigma_{v_3}^2}|\Psi_3(m)|^2\right)\right]\end{aligned} \tag{21}$$

where $\Psi_3(m)$ has been defined in (12), for a given OFDM symbol index n. It is important to note that the first term in the right-hand side (RHS) of (12) is the channel coefficient over the mth subcarrier relative to the direct link between the LTx and the LRx; on the other hand, the second term in the RHS of (12) represents the *backscatter channel* [34] seen by the LRx over the mth subcarrier, which is the concatenation of three components, namely, the forward channel between the LTx and the BTx, the backscatter power wave reflection coefficient, and the backward channel between the BTx and the LRx. Hence, the backscatter channel seen by the LRx experiences *triple* fading due to $\Psi_{12}(m)$, b, and $\Psi_{23}(m)$, which is obviously not Rayleigh.[8] This fact significantly complicates the evaluation of the ensemble average in (21).

A first step towards the analytic computation of C_3 consists of observing that, conditioned on the product $b\,\Psi_{12}(m)$, $|\Psi_3(m)|^2$ turns out to be exponentially distributed with mean $\sigma_{13}^2 + \alpha^2\, \sigma_{23}^2\, |b|^2\, |\Psi_{12}(m)|^2$ ($m \in \mathcal{M}$). Thus, by applying the conditional expectation rule [44], one obtains

$$\mathsf{C}_3 = -\frac{\log e}{M}\sum_{m=0}^{M-1} \mathbb{E}\left\{e^{1/\Upsilon_3(m)}\, \mathrm{Ei}\left[-1/\Upsilon_3(m)\right]\right\} \tag{22}$$

where $\mathrm{Ei}(x) \triangleq \int_{-\infty}^{x} e^u/u\, \mathrm{d}u$ denotes the exponential integral function, for $x < 0$, and

$$\Upsilon_3(m) \triangleq \Gamma_{13}\, \left[1 + \alpha^2\, \frac{\sigma_{23}^2}{\sigma_{13}^2}\, |b|^2\, |\Psi_{12}(m)|^2\right] \tag{23}$$

with $\Gamma_{13} \triangleq (\sigma_{13}^2\, \sigma_s^2)/\sigma_{v_3}^2$ representing the average signal-to-noise ratio (SNR) over the $1 \to 3$ link. When the backscatter system is inactive, i.e., $\alpha = 0$, in accordance with [39], the ergodic capacity of the legacy system is given by

$$\mathsf{C}_3|_{\alpha=0} = -e^{1/\Gamma_{13}}\, \mathrm{Ei}\left(-1/\Gamma_{13}\right)\, \log e\, . \tag{24}$$

A first result can be obtained by comparing (22) and (24). Indeed, since $\Upsilon_3(m) \geq \Gamma_{13}$ for any realizations of $|b|^2$ and $|\Psi_{12}(m)|^2$ and, moreover, $-e^{1/x}\, \mathrm{Ei}(-1/x)$ is a monotonically increasing function of $x \geq 0$, it follows that $\mathsf{C}_3 \geq \mathsf{C}_3|_{\alpha=0}$.

Remark 5: If the constraint (10) on the CP length is satisfied, then backscatter communications can even increase the ergodic capacity of the legacy system. Strictly speaking, the interference generated by the backscatter communication is turned into a form of diversity for the legacy system.

To assess the performance gain $\Delta\mathsf{C}_3 \triangleq \mathsf{C}_3 - \mathsf{C}_3|_{\alpha=0}$, we use asymptotic expressions for C_3 by considering both low- and high-SNR regimes. With this goal in mind, we assume that $\sigma_{ik}^2 = (d_0/d_{ik})^\eta$, where $d_0 > 0$ is a known *reference distance* [36], $d_{ik} \geq d_0$ is the distance between nodes i and k, with $i \neq k$, and η denotes the path-loss exponent. Specifically, since $-e^{1/x}\, \mathrm{Ei}(-1/x) \to x$ as $x \to 0$ [39], in the low-SNR regime, i.e., when $\mathrm{SNR_L} \triangleq \sigma_s^2/\sigma_{v_3}^2 \to 0$, one has

$$\mathsf{C}_3|_{\alpha=0} \to \Gamma_{13}\, \log e \tag{25}$$

and

$$\begin{aligned}\mathsf{C}_3 &\to \frac{\log e}{M}\sum_{m=0}^{M-1} \mathbb{E}[\Upsilon_3(m)] \\ &= \Gamma_{13}\left[1 + \alpha^2\, \sigma_b^2\, \frac{\sigma_{12}^2\, \sigma_{23}^2}{\sigma_{13}^2}\right]\log e\, , \quad \text{for } \mathrm{SNR_L} \to 0\end{aligned} \tag{26}$$

[8]The probability distribution function of the product of Gaussian random variables can be expressed by means of an integral expression, which can be evaluated numerically or by resorting to asymptotic approximations [35].

This article has been accepted for publication in a future issue of this journal, but has not been fully edited. Content may change prior to final publication. Citation information: DOI 10.1109/TCOMM.2017.2654448, IEEE Transactions on Communications

which leads to

$$\Delta \mathsf{C}_3 \to \alpha^2\, \sigma_b^2\, \mathrm{SNR_L} \left(\frac{d_0^2}{d_{12}\, d_{23}}\right)^{\eta} \log e\,, \quad \text{for } \mathrm{SNR_L} \to 0\,. \tag{27}$$

where, according to (5), it results that $\sigma_b^2 = \mathbb{E}(|b|^2) \leq 1$.

On the other hand, by using the asymptotic expression $-e^{1/x}\,\mathrm{Ei}(-1/x) \to \log(1+x) - \gamma$ as $x \to +\infty$ [39], where $\gamma \triangleq \lim_{i\to\infty}\left[i^{-1}\sum_{k=1}^{i} k^{-1} - \log(i)\right] \approx 0.57721$ is the Euler-Mascheroni constant, we have that, in the high-SNR regime, i.e., when $\mathrm{SNR_L} \to +\infty$,

$$\mathsf{C}_3|_{\alpha=0} \to [\log(1+\Gamma_{13}) - \gamma] \log e \tag{28}$$

and, moreover,

$$\mathsf{C}_3 \to \frac{\log e}{M} \sum_{m=0}^{M-1} \mathbb{E}\{\log[1+\Upsilon_3(m)] - \gamma\}, \quad \text{for } \mathrm{SNR_L} \to +\infty. \tag{29}$$

To analytically compute the ensemble average in (29), we assume that the backscatter system employs a constant-modulus constellation, e.g., Q-ary phase-shift keying (PSK), with average energy $\sigma_b^2 = 1$. Henceforth, $|b| = 1$ and, by observing that $|\Psi_{12}(m)|^2$ is exponentially distributed with mean σ_{12}^2, after some calculations, one has

$$\Delta \mathsf{C}_3 \to -e^{1/\Omega_3}\, \mathrm{Ei}\left(-1/\Omega_3\right) \log^2 e\,, \quad \text{for } \mathrm{SNR_L} \to +\infty \tag{30}$$

with

$$\Omega_3 \triangleq \alpha^2\, \frac{\sigma_{23}^2\, \sigma_{12}^2}{\sigma_{13}^2} = \alpha^2 \left(\frac{d_0\, d_{13}}{d_{12}\, d_{23}}\right)^{\eta} \tag{31}$$

where we observed that $\Gamma_{13}/(1+\Gamma_{13}) \to 1$ as $\mathrm{SNR_L} \to +\infty$. Two remarks are now in order.

Remark 6: The capacity gain $\Delta \mathsf{C}_3$ of the legacy system quadratically increases with α^2: the greater the backscatter signal strength, the greater the capacity gain of the legacy system. Such a result comes from the fact that the backscatter device also acts as a non-regenerative relay for the legacy system [37], [38].

Remark 7: With reference to Fig. 1, let η, the angle ϕ between nodes 2 and 3, and the distance d_{13} between the LTx and the LRx be fixed. As a consequence of the Carnot's cosine law, it follows that $d_{23} = (d_{12}^2 + d_{13}^2 - 2\, d_{12}\, d_{13}\, \cos\phi)^{1/2}$, which can be substituted in (27) and (31). By using standard calculus concepts, it is verified that, in both low- and high-SNR regimes, $\Delta \mathsf{C}_3$ is *not* a monotonic function of the distance d_{12} between the LTx and the BTx, for each $\phi \in [0, 2\pi)$. Indeed, it results that $\Delta \mathsf{C}_3$ is a strictly decreasing function of d_{12}/d_{13} when $9\,\cos^2\phi - 8 < 0$, i.e., the angle ϕ belongs to the set

$$\mathcal{A} \triangleq \Big\{\arccos(2\sqrt{2}/3) < a < \pi - \arccos(2\sqrt{2}/3) \text{ and } \pi + \arccos(2\sqrt{2}/3) < a < 2\pi - \arccos(2\sqrt{2}/3)\Big\}\,. \tag{32}$$

In this former case, the capacity gain attains its maximum when the BTx is brought nearer to the LTx and decreases as the BTx moves away from the LTx. On the other hand, when $\phi \notin \mathcal{A}$, i.e., $9\,\cos^2\phi - 8 \geq 0$, the capacity gain $\Delta \mathsf{C}_3$ monotonically increases for $d_{\min}(\phi) \leq d_{12}/d_{13} \leq d_{\max}(\phi)$, with

$$d_{\min}(\phi) \triangleq \max\left(0, \frac{3\,\cos\phi - \sqrt{9\,\cos^2\phi - 8}}{4}\right) \tag{33}$$

$$d_{\max}(\phi) \triangleq \max\left(0, \frac{3\,\cos\phi + \sqrt{9\,\cos^2\phi - 8}}{4}\right) \tag{34}$$

otherwise, it monotonically decreases. In this latter case, the capacity gain of the legacy system tends to assume a maximum when the BTx gets closer and closer to the LTx, and exhibits a minimum and another maximum at $d_{\min}(\phi)$ and $d_{\max}(\phi)$, respectively. For instance, if LTx, BTx, and LRx lie on the same line, i.e., $\phi = 0$, the gain $\Delta \mathsf{C}_3$ monotonically decreases for $0 < d_{12}/d_{13} \leq 1/2$ and $d_{12}/d_{13} > 1$, while it increases when $1/2 < d_{12}/d_{13} < 1$.

If no significant channel variability occurs during the whole legacy transmission (i.e., the transmission duration of the codeword is comparable to the channel coherence time), a capacity in the ergodic sense does not exist. In this case, the concept of *capacity versus outage* has to be used [33], [39]. Assuming that codewords extend over a single legacy symbol and that the LTx encode data at a rate of R_s b/s/Hz, the outage probability of the legacy system is defined as

$$\mathsf{P}_{\text{out},3} \triangleq P\left\{\frac{1}{M}\sum_{m=0}^{M-1} \log\left[1 + \frac{\sigma_s^2}{\sigma_{v_3}^2}|\Psi_3(m)|^2\right] < R_s\right\}\,. \tag{35}$$

However, for the problem at hand, $\mathsf{P}_{\text{out},3}$ is hard to compute analytically and does not lead to easily interpretable results. Therefore, we resort to numerical simulations presented in Section V to show the influence of the main system parameters on the outage probability of the legacy transmission.

IV. Capacity analysis of the backscatter system

To keep the analysis of the backscatter system relatively simple from a mathematical viewpoint, we remove the IBI in (17) by replacing condition (15) with the following one

$$L_b \geq \max\left(L_{14} + \theta_{14}, L_{24} + \theta_{24}, L_{12} + L_{24} + \theta_{12} + \theta_{24}\right)\,. \tag{36}$$

Inequality (36) imposes further restrictions on both network size and time dispersivity of the channels. Under the assumption that

$$L_{12} + L_{24} + \theta_{12} + \theta_{24} \leq P - 1 \tag{37}$$

since only the first $L_{12} + L_{24} + \theta_{12} + \theta_{24}$ rows of $\widetilde{\mathbf{C}}_{24}^{(0)}\, \widetilde{\mathbf{C}}_{12}^{(1)}$ might not be zero, one thus has $\mathbf{R}_b\, \mathbf{\Sigma}_\nu\, \widetilde{\mathbf{C}}_{24}^{(0)}\, \widetilde{\mathbf{C}}_{12}^{(1)} = \mathbf{O}_{N\times P}$. Obviously, removing the IBI in (17) is not the best choice, since it does not allow one to exploit the entire channel energy. However, such a contribution becomes negligible for large values of N (i.e., P). Moreover, we assume herein that the number of samples L_b discarded from the received backscatter signal (14) is just equal to L_{cp}. We note that, when $L_{\text{cp}} = L_b$, then $N = M$ in (16)–(18). In this case, if (9) holds, the product $\widetilde{\mathbf{C}}_{24}^{(0)}\, \widetilde{\mathbf{C}}_{12}^{(0)}$ is a lower-triangular Toeplitz matrix having as first column $[\mathbf{0}_{\theta_{12}+\theta_{24}}^{\mathrm{T}}, \mathbf{c}_{124}^{\mathrm{T}}, \mathbf{0}_{P-L_{12}-L_{24}-\theta_{12}-\theta_{24}-1}^{\mathrm{T}}]^{\mathrm{T}}$, where the vector $\mathbf{c}_{124} \in \mathbb{C}^{L_{12}+L_{24}+1}$ collects the samples of the

This article has been accepted for publication in a future issue of this journal, but has not been fully edited. Content may change prior to final publication. Citation information: DOI 10.1109/TCOMM.2017.2654448, IEEE Transactions on Communications

(linear) convolution between $\{c_{12}(\ell)\}_{\ell=0}^{L_{12}}$ and $\{c_{24}(\ell)\}_{\ell=0}^{L_{24}}$. In the forthcoming subsections, we separately consider the two different network configurations depicted in Fig. 1.

A. The BRx and LTx are co-located

When the intended recipient of the backscatter signal and the legacy transmitter are co-located on the same device (see the left-side plot of Fig. 1), the reference signal model can be obtained from (16)–(18) and (36)–(37) by replacing the subscript 4 with 1 and setting $\nu = 0$. In this case, the symbol vector $\mathbf{s}(n)$ [and, thus, $\mathbf{u}(n)$] is perfectly known at the LTRx, whereas the parameters $\{\mathbf{c}_{121}, \theta_{12} + \theta_{21}\}$, which uniquely identify the matrix $\widetilde{\mathbf{C}}_{21}^{(0)}\,\widetilde{\mathbf{C}}_{12}^{(0)}$, and $\{\mathbf{c}_{11}, \theta_{11}\}$, which uniquely identify the matrix $\widetilde{\mathbf{C}}_{11}^{(0)}$, with $\mathbf{c}_{11} \triangleq [c_{11}(0), c_{11}(1), \ldots, c_{11}(L_{11})]^{\mathrm{T}} \in \mathbb{C}^{L_{11}+1}$, can be estimated by allowing the insertion of training data within each packet of B symbols transmitted by the BTx. More precisely, the self-interference parameters $\{\mathbf{c}_{11}, \theta_{11}\}$ can be estimated when there is no backscatter transmission, by employing a *silent period* of few symbols at the beginning of the packet [6], during which the BTx does not backscatter (i.e., $\alpha = 0$). Once $\mathbf{c}_{11}$ and θ_{11} have been estimated by means of standard techniques [40], the self-interference contribution can be subtracted from (16). After the silent period, the BTx modulates training symbols on the backscatter signal [6], which can be used to estimate $\{\mathbf{c}_{121}, \theta_{12} + \theta_{21}\}$ through conventional methods [40]. After performing the DFT, one gets

$$\begin{aligned}\mathbf{r}_1(n) &\triangleq \mathbf{W}_{\mathrm{DFT}}\,\mathbf{R}_b\left[\widetilde{\mathbf{r}}_1(n) - \widetilde{\mathbf{C}}_{11}^{(0)}\,\mathbf{u}(n)\right] \\ &= \alpha\,\boldsymbol{\psi}(n)\,b(n) + \mathbf{v}_1(n)\end{aligned} \tag{38}$$

where $\mathbf{W}_{\mathrm{DFT}} \triangleq \mathbf{W}_{\mathrm{IDFT}}^{-1} = \mathbf{W}_{\mathrm{IDFT}}^{\mathrm{H}}$ defines the unitary symmetric DFT matrix [16], the vector $\boldsymbol{\psi}(n) \triangleq \boldsymbol{\Psi}_{12}\,\boldsymbol{\Psi}_{21}\,\mathbf{s}(n) \in \mathbb{C}^M$ is the backscatter channel seen by the LTRx, the nonzero entries of the matrix

$$\boldsymbol{\Psi}_{ik} \triangleq \mathrm{diag}[\Psi_{ik}(0), \Psi_{ik}(1), \ldots, \Psi_{ik}(M-1)] \tag{39}$$

are given by (13), and $\mathbf{v}_1(n) \triangleq \mathbf{W}_{\mathrm{DFT}}\,\mathbf{R}_b\,\widetilde{\mathbf{v}}_1(n) \in \mathbb{C}^M$. Due to the concatenation of $\boldsymbol{\Psi}_{12}$, $\boldsymbol{\Psi}_{21}$, and $\mathbf{s}(n)$, the vector $\boldsymbol{\psi}(n)$ is not normally distributed. On the basis of the above discussion, the vector $\boldsymbol{\psi}(n)$ is assumed to be known at the LTRx and, thus, *coherent* receiving rules can be adopted at the LTRx. Moreover, we will omit the dependence on the symbol index n hereinafter.

According to (38), given $\boldsymbol{\psi}$, a sufficient statistic for detecting b from $\mathbf{r}_1$ is given by the scalar

$$z_1 \triangleq \boldsymbol{\psi}^{\mathrm{H}}\,\mathbf{r}_1 = \alpha\,\|\boldsymbol{\psi}\|^2\,b + \boldsymbol{\psi}^{\mathrm{H}}\,\mathbf{v}_1\,. \tag{40}$$

Since sufficient statistics preserve mutual information [31], [32], one has $\mathsf{I}(b; \mathbf{r}_1, \boldsymbol{\psi}) = \mathsf{I}(b; z_1, \boldsymbol{\psi})$. Therefore, the coherent ergodic capacity of (38) is given by

$$\mathsf{C}_1 \triangleq \sup_{f(b)\in\mathcal{I}_b} \frac{\mathsf{I}(b; z_1, \boldsymbol{\psi})}{M} \quad \text{(in b/s/Hz)} \tag{41}$$

where $\mathcal{I}_b$ is the set of admissible input distributions $f(b)$ fulfilling *both* the variance constraint $\mathbb{E}(|b|^2) = \sigma_b^2$ and, according to (5), the amplitude constraint $|b| \leq 1$ almost surely (a.s.). Since the average of a random variable cannot exceed its maximal value, the amplitude constraint implies that $\sigma_b^2 \leq 1$.

We observe that (40) is a conditionally Gaussian channel, given b and $\boldsymbol{\psi}$. It was shown in [41] that the capacity-achieving input distribution for conditional Gaussian channels under variance and amplitude constraints is *discrete* with a *finite* number of mass points. Therefore, there is no loss of generality in confining $f(b)$ to the set of discrete distributions. To this goal, let b be a discrete random variable taking on the value $\beta_q \in \mathcal{B}$ with probability p_q, for each $q \in \mathcal{Q}$, such that $|\beta_q| \leq 1$, $\mathbb{E}(|b|^2) = \sigma_b^2$, and $\sum_{q\in\mathcal{Q}} p_q = 1$. Using the same arguments of Subsection III, one gets

$$\mathsf{I}(b; z_1, \boldsymbol{\psi}) = \mathsf{I}(b; z_1 \,|\, \boldsymbol{\psi}) = \mathbb{E}_{\boldsymbol{\psi}}\left[\mathsf{I}(b; z_1 \,|\, \boldsymbol{\psi} = \boldsymbol{\xi})\right] \tag{42}$$

where the entries of the backscatter channel $\boldsymbol{\psi}$ are not Gaussian due to the concatenation of $\boldsymbol{\Psi}_{12}$, $\boldsymbol{\Psi}_{21}$, and $\mathbf{s}$. For the discrete input b, the mutual information $\mathsf{I}(b; z_1 \,|\, \boldsymbol{\psi} = \boldsymbol{\xi})$ is given by

$$\mathsf{I}(b; z_1 \,|\, \boldsymbol{\psi} = \boldsymbol{\xi}) = \mathsf{h}(z_1 \,|\, \boldsymbol{\psi} = \boldsymbol{\xi}) - \mathsf{h}(z_1 \,|\, b, \boldsymbol{\psi} = \boldsymbol{\xi}) \tag{43}$$

where

$$\mathsf{h}(z_1 \,|\, \boldsymbol{\psi} = \boldsymbol{\xi}) = -\int f_{z_1\,|\,\boldsymbol{\psi}=\boldsymbol{\xi}}(x)\,\log f_{z_1\,|\,\boldsymbol{\psi}=\boldsymbol{\xi}}(x)\,\mathrm{d}x \tag{44}$$

is the differential entropy [31], [32] of $z_1 \,|\, \boldsymbol{\psi} = \boldsymbol{\xi}$, whereas

$$\begin{aligned}\mathsf{h}(z_1 \,|\, b, \boldsymbol{\psi} = \boldsymbol{\xi}) &= \mathsf{h}(\alpha\,\|\boldsymbol{\psi}\|^2\,b + \boldsymbol{\psi}^{\mathrm{H}}\,\mathbf{v}_1 \,|\, b, \boldsymbol{\psi} = \boldsymbol{\xi}) \\ &= \mathsf{h}(\boldsymbol{\psi}^{\mathrm{H}}\,\mathbf{v}_1 \,|\, b, \boldsymbol{\psi} = \boldsymbol{\xi}) = \mathsf{h}(\boldsymbol{\xi}^{\mathrm{H}}\,\mathbf{v}_1)\end{aligned} \tag{45}$$

turns out to be the differential entropy of $\boldsymbol{\xi}^{\mathrm{H}}\,\mathbf{v}_1 \sim \mathcal{CN}(0, \sigma_{v_1}^2\|\boldsymbol{\xi}\|^2)$, which is given (see, e.g., [42]) by $\mathsf{h}(\boldsymbol{\xi}^{\mathrm{H}}\,\mathbf{v}_1) = \log(\pi e\,\mathbb{E}[|\boldsymbol{\xi}^{\mathrm{H}}\,\mathbf{v}_1|^2])$. It is noteworthy that, given $\boldsymbol{\psi} = \boldsymbol{\xi}$, the output distribution

$$f_{z_1\,|\,\boldsymbol{\psi}=\boldsymbol{\xi}}(x) = \sum_{q=1}^{Q} p_q\,f_{z_1\,|\,b=\beta_q,\boldsymbol{\psi}=\boldsymbol{\xi}}(x) \tag{46}$$

is a Gaussian mixture since $z_1 \,|\, b = \beta_q, \boldsymbol{\psi} = \boldsymbol{\xi} \sim \mathcal{CN}(\alpha\,\|\boldsymbol{\xi}\|^2\,\beta_q, \sigma_{v_1}^2\|\boldsymbol{\xi}\|^2)$. By virtue of (43), the optimization problem (41) is equivalent to the supremization of $\mathbb{E}_{\boldsymbol{\psi}}[\mathsf{h}(z_1 \,|\, \boldsymbol{\psi} = \boldsymbol{\xi})]$ under the variance and amplitude constraints. However, the entropy $\mathsf{h}(z_1 \,|\, \boldsymbol{\psi} = \boldsymbol{\xi})$ cannot be calculated in closed form due to the logarithm of a sum of exponential functions. As a consequence, an analytical expression for the optimizing probability mass function (pmf) of b is not available for the general case, neither there exists a closed-form formula for the corresponding capacity. Henceforth, upper and lower bounds on C_1 given by (41) are developed in the sequel.

An upper bound on C_1 can be obtained by resorting to the maximum-entropy theorem for complex random variables [42], which allows one to state that

$$\begin{aligned}\mathsf{h}(z_1 \,|\, \boldsymbol{\psi} = \boldsymbol{\xi}) &\leq \log\left(\pi e\,\mathbb{E}\left[|z_1|^2 \,\middle|\, \boldsymbol{\psi} = \boldsymbol{\xi}\right]\right) \\ &= \log\left(\alpha^2\,\sigma_b^2\,\|\boldsymbol{\xi}\|^4 + \sigma_{v_1}^2\,\|\boldsymbol{\xi}\|^2\right)\,.\end{aligned} \tag{47}$$

By substituting (47) in (43) and accounting for (41)–(42), one gets the upper bound

$$\mathsf{C}_1 \leq \mathsf{C}_{1,\mathrm{upper}} \triangleq \frac{1}{M}\,\mathbb{E}\left[\log\left(1 + \mathrm{SNR}_{\mathrm{B},1}\,\Theta_{121}\right)\right] \tag{48}$$

This article has been accepted for publication in a future issue of this journal, but has not been fully edited. Content may change prior to final publication. Citation information: DOI 10.1109/TCOMM.2017.2654448, IEEE Transactions on Communications

with $\mathrm{SNR}_{\mathrm{B},1} \triangleq \alpha^2 \sigma_b^2 / \sigma_{v_1}^2$ and

$$\Theta_{121} \triangleq \sum_{m=0}^{M-1} |s^{(m)}|^2 \, |\Psi_{12}(m)|^2 |\Psi_{21}(m)|^2 \, . \tag{49}$$

It can be shown that, as Q grows, C_1 approaches $\mathsf{C}_{1,\mathrm{upper}}$ exponentially fast [43]. In the general case, the evaluation of the expectation in (48) is significantly complicated and will be numerically carried out in Section V. Herein, we shall resort to a simpler asymptotic analysis by assuming that M is sufficiently large. It follows from the law of large numbers [44] that, as M gets large, the random variable Θ_{121}/M converges a.s. to $\sigma_s^2 \, \sigma_{12}^2 \, \sigma_{21}^2$. Hence, observing that, according to the considered path-loss model, it results that $\sigma_{12}^2 = \sigma_{21}^2$ since $d_{12} = d_{21}$, in the large M limit, one can write[9]

$$\begin{aligned} \mathsf{C}_1 \leq \mathsf{C}_{1,\mathrm{upper}}|_{M \gg 1} &\triangleq \frac{1}{M} \, \log \left(1 + \mathrm{SNR}_{\mathrm{B},1} \, M \, \sigma_s^2 \, \sigma_{12}^4\right) \\ &= \frac{1}{M} \, \log \left[1 + \mathrm{SNR}_{\mathrm{B},1} \, M \, \sigma_s^2 \left(\frac{d_0^2}{d_{12}^2}\right)^{\eta}\right] . \end{aligned} \tag{50}$$

Remark 8: When M is sufficiently large, the upper bound (48) is a monotonically increasing function of $\mathrm{SNR}_{\mathrm{B},1}$ and $1/d_{12}$. In other words, higher values of C_1 are obtained when the BTx reflects a large part of the incident EM wave and/or the BTx is very close to the LTRx.

A lower bound on C_1 is developed in Appendix A as reported at the top of the next page in (51). The further lower bound

$$\mathsf{C}_{1,\mathrm{lower}} \geq \frac{\log Q - \mathbb{E}\left\{\log\left[1 + (Q-1)\, e^{-\Theta_{121}\, \mathrm{SNR}_{\mathrm{B},1} \, \frac{\delta_{\min}^2}{4\,\sigma_b^2}}\right]\right\}}{M} \tag{52}$$

can be obtained by noting that $|\beta_1 - \beta_q|^2 \geq \delta_{\min}^2$ for each $q \in \mathcal{Q}$, where $\delta_{\min} \triangleq \min_{q_1 \neq q_2 \in \mathcal{Q}} |\beta_{q_1} - \beta_{q_2}|$ is the minimum distance between any two data symbols in the signal constellation $\mathcal{B}$. By invoking again the law of large numbers [44], in the large M limit, one has the asymptotic expressions of $\mathsf{C}_{1,\mathrm{lower}}$ and its lower bound (52) as reported at the top of the next page in (53).

Remark 9: The lower bound $\mathsf{C}_{1,\mathrm{lower}}$ approaches $(\log Q)/M$ if $\mathrm{SNR}_{\mathrm{B},1}$ is sufficiently large and the distance d_{12} is comparable to d_0. On the other hand, when $x \to 0$, the function $\log(1 + A\, e^{-Bx})$ can be approximated using the first two terms of its Mac Laurin series expansion, i.e., $\log(1 + A\, e^{-B\,x}) \approx \log(1+A) - A\,B\,(1+A)^{-1} x$, hence getting

$$\mathsf{C}_{1,\mathrm{lower}|_{M \gg 1}} \to \left(1 - \frac{1}{Q}\right) \frac{\sigma_s^2 \, \mathrm{SNR}_{\mathrm{B},1} \, \delta_{\min}^2}{4\,\sigma_b^2} \left(\frac{d_0^2}{d_{12}^2}\right)^{\eta} \tag{54}$$

in the low-SNR regime $\mathrm{SNR}_{\mathrm{B},1} \to 0$ and/or when $d_0/d_{12} \to 0$: in this case, the capacity increases linearly with $\mathrm{SNR}_{\mathrm{B},1}$ and monotonically decreases as the distance d_{12} raises.

[9]For any value of M, eq. (50) is as an upper bound on (48): indeed, by virtue of the Jensen's inequality, one has $\mathbb{E}[\log(1 + \mathrm{SNR}_{\mathrm{B},1}\, \Theta_{121})] \leq \log[1 + \mathrm{SNR}_{\mathrm{B},1}\, \mathbb{E}(\Theta_{121})]$, with $\mathbb{E}(\Theta_{121}) = M\, \sigma_s^2 \, \sigma_{12}^2 \, \sigma_{21}^2$.

B. The BRx and LTx are spatially-separated nodes

We consider the scenario where the LTx and BRx are spatially-separated nodes (see the right-side plot of Fig. 1). In this case, taking into account the aforementioned simplifying assumptions (36) and $L_{\mathrm{cp}} = L_b$, the reference signal model (16)–(18) becomes

$$\mathbf{R}_b \, \widetilde{\mathbf{r}}_4(n) = \alpha \left[e^{j\frac{2\pi}{M}\nu n P} \, \mathbf{R}_b \, \mathbf{\Sigma}_\nu \, \widetilde{\mathbf{C}}_{24}^{(0)} \, \widetilde{\mathbf{C}}_{12}^{(0)} \, \mathbf{u}(n)\right] b(n) + \mathbf{d}_4(n) \tag{55}$$

with

$$\mathbf{d}_4(n) = e^{j\frac{2\pi}{M}\nu n P} \, \mathbf{R}_b \, \mathbf{\Sigma}_\nu \, \widetilde{\mathbf{C}}_{14}^{(0)} \, \mathbf{u}(n) + \mathbf{R}_b \, \widetilde{\mathbf{v}}_4(n) \in \mathbb{C}^M . \tag{56}$$

We note that the overall backscatter channel seen by the BRx is given by $e^{j\frac{2\pi}{M}\nu n P} \, \mathbf{R}_b \, \mathbf{\Sigma}_\nu \, \widetilde{\mathbf{C}}_{24}^{(0)} \, \widetilde{\mathbf{C}}_{12}^{(0)} \, \mathbf{u}(n)$ and experiences non-Rayleigh triple fading due to the concatenation of $\widetilde{\mathbf{C}}_{24}^{(0)}$, $\widetilde{\mathbf{C}}_{12}^{(0)}$, and $\mathbf{u}(n)$. Compared to the case studied in Subsection IV-A, there are two key differences: (i) the receiver has no knowledge of the data block $\mathbf{u}(n)$ transmitted by the LTx and, thus, the interference arising from the legacy transmission along the $1 \to 4$ link cannot be simply subtracted from (55); (ii) there is a nonzero CFO ν between the received carrier and the local sinusoids used for signal demodulation.

If the BRx does not have any *a priori* knowledge regarding the legacy transmission, recovery of $b(n)$ can be accomplished at the BRx by resorting to *noncoherent* detection rules. The noncoherent ergodic capacity of (55)–(56) is given by the supremum of the mutual information $\mathsf{I}[b; \mathbf{R}_b \, \widetilde{\mathbf{r}}_4(n)]$ over the set $\mathcal{I}_b$ of admissible input distribution satisfying both the variance and amplitude constraints. Evaluation of the noncoherent ergodic capacity with only a variance constraint has been studied in [46], [47], [48] under the assumption that the channel matrix [corresponding to $e^{j\frac{2\pi}{M}\nu n P} \, \mathbf{R}_b \, \mathbf{\Sigma}_\nu \, \widetilde{\mathbf{C}}_{24}^{(0)} \, \widetilde{\mathbf{C}}_{12}^{(0)} \, \mathbf{u}(n)$ in our framework] and noise [corresponding to $\mathbf{d}_4(n)$ in our framework] follow a Gaussian distribution. In the case under study, evaluation of the noncoherent ergodic capacity is further complicated by the non-Gaussian nature of both $e^{j\frac{2\pi}{M}\nu n P} \, \mathbf{R}_b \, \mathbf{\Sigma}_\nu \, \widetilde{\mathbf{C}}_{24}^{(0)} \, \widetilde{\mathbf{C}}_{12}^{(0)} \, \mathbf{u}(n)$ and $\mathbf{d}_4(n)$, as well as by the amplitude constraint $|b| \leq 1$.

To provide an upper-bound benchmark for the performance of noncoherent backscatter communications, we study the case where, besides having knowledge of the training symbols transmitted by the BTx, the BRx additionally knows the pilot symbols sent by the LTx in each OFDM symbol. Such an assumption is realistic in those applications where the BTx and BRx are not paired up opportunistically, but instead they operate in a planned fashion with the legacy system, e.g., D2D-enabled cellular networks [3]. In this case, following the same protocol outlined in Subsubsection IV-A, during the silent period of the BTx (i.e., when $\alpha = 0$), the BRx receives the signal $\mathbf{d}_4(n)$, from which it can estimate the CFO ν and the parameters of the channel matrix $\widetilde{\mathbf{C}}_{14}^{(0)}$ by resorting to standard estimators [28], [40]. However, it should be observed that the interference contribution $e^{j\frac{2\pi}{M}\nu n P} \, \mathbf{R}_b \, \mathbf{\Sigma}_\nu \, \widetilde{\mathbf{C}}_{14}^{(0)} \, \mathbf{u}(n)$ cannot be subtracted from (55) since the information-bearing data in $\mathbf{u}(n)$ are unknown at the BRx (only the pilots and their locations are assumed to be known). Once ν has been

This article has been accepted for publication in a future issue of this journal, but has not been fully edited. Content may change prior to final publication. Citation information: DOI 10.1109/TCOMM.2017.2654448, IEEE Transactions on Communications

$$\mathsf{C}_1 \geq \mathsf{C}_{1,\text{lower}} \triangleq \frac{\log Q - \mathbb{E}\left[\log\left(1+\sum_{q=2}^{Q} e^{-\Theta_{121}\,\text{SNR}_{\text{B},1}\,\frac{|\beta_1-\beta_q|^2}{4\,\sigma_b^2}}\right)\right]}{M} \tag{51}$$

$$\mathsf{C}_{1,\text{lower}|_{M\,\gg\,1}} \triangleq \frac{\log Q - \log\left[1+\sum_{q=2}^{Q} e^{-\frac{\sigma_s^2\,M\,\text{SNR}_{\text{B},1}\,|\beta_1-\beta_q|^2}{4\,\sigma_b^2}\left(\frac{d_0^2}{d_{12}^2}\right)^{\eta}}\right]}{M} \geq \frac{\log Q - \log\left[1+(Q-1)\,e^{-\frac{\sigma_s^2\,M\,\text{SNR}_{\text{B},1}\,\delta_{\min}^2}{4\,\sigma_b^2}\left(\frac{d_0^2}{d_{12}^2}\right)^{\eta}}\right]}{M} \tag{53}$$

estimated, the vector $\widetilde{\mathbf{r}}_4(n)$ is counter-rotated at the angular speed $2\pi\nu/M$, thus yielding

$$\mathbf{r}_4 \triangleq \mathbf{R}_b\,\widetilde{\mathbf{r}}_4 = \alpha\,(\mathbf{W}_{\text{IDFT}}\,\mathbf{\Psi}_{12}\,\mathbf{\Psi}_{24}\,\mathbf{s})\,b + \mathbf{W}_{\text{IDFT}}\,\mathbf{\Psi}_{14}\,\mathbf{s} + \mathbf{v}_4 \tag{57}$$

with $\mathbf{v}_4 \triangleq \mathbf{R}_b\,\widetilde{\mathbf{v}}_4 \in \mathbb{C}^M$, where $\mathbf{s} \sim \mathcal{CN}(\mathbf{0}_M, \sigma_s^2\,\mathbf{I}_M)$ is the capacity-achieving distribution for the legacy system (see Section III) and we have again omitted the dependence of the symbol index n. Since $\mathbf{\Omega}_{124} \triangleq \mathbf{\Psi}_{12}\,\mathbf{\Psi}_{24} \in \mathbb{C}^{M\times M}$ and $\mathbf{\Omega}_{14} \triangleq \mathbf{\Psi}_{14} \in \mathbb{C}^{M\times M}$ are known but $\mathbf{s}$ is unknown, we refer to (57) as the *partially-coherent* channel model. The partially-coherent ergodic capacity of (57) is given by

$$\mathsf{C}_4 \triangleq \sup_{f(b)\in\mathcal{I}_b} \mathsf{I}(b;\mathbf{r}_4,\mathbf{\Omega}_{124},\mathbf{\Omega}_{14}) \tag{58}$$

where $\mathcal{I}_b$ is the set of admissible input distributions fulfilling $\mathbb{E}(|b|^2) = \sigma_b^2$ and $|b| \leq 1$ a.s., and

$$\begin{aligned}\mathsf{I}(b;\mathbf{r}_4,\mathbf{\Omega}_{124},\mathbf{\Omega}_{14}) &= \mathsf{I}(b;\mathbf{r}_4\,|\,\mathbf{\Omega}_{124},\mathbf{\Omega}_{14})\\ &= \mathbb{E}_{\mathbf{\Omega}_{124},\mathbf{\Omega}_{14}}\left[\mathsf{I}(b;\mathbf{r}_4\,|\,\mathbf{\Omega}_{124}=\mathbf{\Xi}_{124},\mathbf{\Omega}_{14}=\mathbf{\Xi}_{14})\right]\,.\end{aligned} \tag{59}$$

Similarly to the case studied in Subsection IV-A, closed-form expressions for C_4 and for the capacity-achieving discrete distribution $f(b)$ are unavailable. Therefore, we derive upper and lower bounds on C_4.

An upper bound on C_4 is obtained in Appendix B by assuming that the BRx has the additional knowledge of $\mathbf{s}$, thus yielding

$$\mathsf{C}_4 \leq \mathsf{C}_{4,\text{upper}} \triangleq \frac{1}{M}\,\mathbb{E}\left[\log\left(1+\text{SNR}_{\text{B},4}\,\Theta_{124}\right)\right] \tag{60}$$

with $\text{SNR}_{\text{B},4} \triangleq \alpha^2\sigma_b^2/\sigma_{v_4}^2$ and

$$\Theta_{124} \triangleq \sum_{m=0}^{M-1} |s^{(m)}|^2\,|\Psi_{12}(m)|^2|\Psi_{24}(m)|^2\,. \tag{61}$$

Such an upper bound is achieved when the BRx is able to reliably estimate the legacy symbols, which allows one to counteract the interference generated by the legacy transmission over the $1\to 4$ link, and $Q\to+\infty$. It should be noted that (60) is similar to (48). Thus, the asymptotic analysis reported in Subsection IV-A soon after (48) can be applied to (60) with minor modifications. In particular, in the large M limit, one obtains

$$\begin{aligned}\mathsf{C}_4 \leq \mathsf{C}_{4,\text{upper}}|_{M\,\gg\,1} &\triangleq \frac{1}{M}\,\log\left(1+\text{SNR}_{\text{B},4}\,M\,\sigma_s^2\,\sigma_{12}^2\,\sigma_{24}^2\right)\\ &= \frac{1}{M}\,\log\left[1+\text{SNR}_{\text{B},4}\,M\,\sigma_s^2\left(\frac{d_0^2}{d_{12}\,d_{24}}\right)^{\eta}\right]\end{aligned} \tag{62}$$

where, by virtue of the Carnot's cosine law, one has $d_{24} = (d_{12}^2+d_{14}^2-2\,d_{12}\,d_{14}\,\cos\theta)^{1/2}$, with θ being the angle opposite to the $2\to 4$ link (see the right-side plot of Fig. 1).

Remark 10: For a fixed value of η, d_{14}, and θ, the capacity $\mathsf{C}_{4,\text{upper}}|_{M\,\gg\,1}$ as a function of d_{12} exhibits the same behavior of $\Delta\mathsf{C}_3$ (see Remark 7). In a nutshell, when $\theta\in\mathcal{A}$, the upper bound $\mathsf{C}_{4,\text{upper}}|_{M\,\gg\,1}$ attains its maximum when the BTx gets close to LTx and decreases while the BTx is departing from the LTx; on the other hand, when $\theta\notin\mathcal{A}$, it results that $\mathsf{C}_{4,\text{upper}}|_{M\,\gg\,1}$ tends to assume a maximum as the BTx approaches the LTx and exhibits a minimum and another maximum at $d_{\min}(\theta)$ and $d_{\max}(\theta)$, respectively.

The lower bound on C_4, which is reported at the top of the next page in (63), is derived in Appendix C, with

$$\begin{aligned}\Lambda_q(m) \triangleq\; &\alpha^2\,\sigma_s^2\,|\Psi_{12}(m)|^2\,|\Psi_{24}(m)|^2\,|\beta_q|^2\\ &+2\,\alpha\,\sigma_s^2\,\Re\left\{\Psi_{12}(m)\,\Psi_{24}(m)\,\Psi_{14}^*(m)\,\beta_q\right\}\\ &+\sigma_s^2\,|\Psi_{14}(m)|^2+\sigma_{v_4}^2\,.\end{aligned} \tag{64}$$

As previously anticipated, in addition to noise, another additive source of performance degradation is the interference generated by the legacy system over the $1\to 4$ link, which may limit the worst-case achievable rates of the backscatter system in the high-SNR region.

Remark 11: It is verified from (63) that $\mathsf{C}_{4,\text{lower}}\to 0$ if $\Lambda_{q_1}(m)\to\Lambda_{q_2}(m)$ for each $q_1\neq q_2\in\mathcal{Q}$. For instance, this happens when the second and third summands in the RHS of (64) are dominant over the first and second ones, i.e., when interference and/or noise dominates the backscatter signal.

The dependence of the $\mathsf{C}_{4,\text{lower}}$ on the distance d_{12} between the LTx and the BTx is not easily deduced from (63) and such a behavior is studied numerically in Section V. To gain some useful insights, we consider the special case of a 2-PSK (i.e., BPSK), where $\beta_1=-\beta_2=1$. In this case, eq. (63) becomes

$$\mathsf{C}_{4,\text{lower}}^{\text{bpsk}} = \frac{1}{M} - \frac{1}{M}\,\mathbb{E}\left\{\log\left[1+\prod_{m=0}^{M-1}\sqrt{1-\frac{\Lambda_1^2(m)}{\Lambda_2^2(m)}}\right]\right\}$$

This article has been accepted for publication in a future issue of this journal, but has not been fully edited. Content may change prior to final publication. Citation information: DOI 10.1109/TCOMM.2017.2654448, IEEE Transactions on Communications

$$\mathsf{C}_4 \geq \mathsf{C}_{4,\text{lower}} \triangleq \frac{\log Q - \mathbb{E}\left[\log\left(1 + \frac{2^M}{Q}\sum_{q_1=1}^{Q}\sum_{\substack{q_2=1\\ q_2\neq q_1}}^{Q}\prod_{m=0}^{M-1}\frac{\sqrt{\Lambda_{q_1}(m)\,\Lambda_{q_2}(m)}}{\Lambda_{q_1}(m)+\Lambda_{q_2}(m)}\right)\right]}{M} \tag{63}$$

$$\geq \frac{1}{M} - \frac{1}{M}\,\log\left\{1+\sqrt{\mathbb{E}\left[\prod_{m=0}^{M-1}\left(1-\frac{\Lambda_1^2(m)}{\Lambda_2^2(m)}\right)\right]}\right\}$$
$$\approx \frac{1}{M} - \frac{1}{M}\,\log\left\{1+\sqrt{\prod_{m=0}^{M-1}\left(1-\mathbb{E}\left[\frac{\Lambda_1^2(m)}{\Lambda_2^2(m)}\right]\right)}\right\} \tag{65}$$

with

$$\Lambda_1(m) \triangleq \alpha^2\,\sigma_s^2\,|\Psi_{12}(m)|^2\,|\Psi_{24}(m)|^2 + \sigma_s^2\,|\Psi_{14}(m)|^2 + \sigma_{v_4}^2 \tag{66}$$

$$\Lambda_2(m) \triangleq 2\,\alpha\,\sigma_s^2\,\Re\left\{\Psi_{12}(m)\,\Psi_{24}(m)\,\Psi_{14}^*(m)\right\} \tag{67}$$

where the inequality in (65) comes from the application of the Jensens's inequality to the concave function $\log(1+\sqrt{x})$, whereas the approximation is obtained by neglecting the correlation between the random variables $\Lambda_1^2(m_1)/\Lambda_2^2(m_1)$ and $\Lambda_1^2(m_2)/\Lambda_2^2(m_2)$, for $m_1 \neq m_2 \in \mathcal{M}$. The first-order Taylor expansion of $\mathbb{E}\left[\Lambda_1^2(m)/\Lambda_2^2(m)\right]$ leads to the further approximation[10] $\mathbb{E}\left[\Lambda_1^2(m)/\Lambda_2^2(m)\right] \approx \mathbb{E}[\Lambda_1^2(m)]/\mathbb{E}[\Lambda_2^2(m)]$, where in the low-noise regime $\sigma_{v_4}^2/\sigma_s^2 \to 0$, one has

$$J \triangleq \lim_{\sigma_{v_4}^2/\sigma_s^2\to 0}\frac{\mathbb{E}[\Lambda_1^2(m)]}{\mathbb{E}[\Lambda_2^2(m)]} = \frac{1}{1+\frac{2}{D}+D} \tag{68}$$

where $D \triangleq \left[(d_{12}\,d_{24})/(d_0\,d_{14})\right]^\eta/\alpha^2$ is independent of m, with $d_{24} = (d_{12}^2 + d_{14}^2 - 2\,d_{12}\,d_{14}\,\cos\theta)^{1/2}$. Since $d_{12}, d_{24} \geq d_0$, it results that $D \geq (d_0/d_{14})^\eta/\alpha^2$, which is greater than zero for finite values of d_{14}. Therefore, when $\sigma_{v_4}^2/\sigma_s^2 \to 0$, it results from (65) that[11]

$$\mathsf{C}_{4,\text{lower}}^{\text{bpsk}} \gtrsim \frac{1}{M} - \frac{1}{M}\,\log\left[1+(1-J)^{M/2}\right]. \tag{69}$$

Remark 12: $0 < J < 1$ is a unimodal function of D exhibiting a maximum when $D = \sqrt{2}$. However, if α is much smaller than one and the network size is small (e.g., indoor scenario), then D takes on values greater than $\sqrt{2}$ and J decreases as D increases. Therefore, the capacity $\mathsf{C}_{4,\text{lower}}^{\text{bpsk}}$ is an increasing function of $1/D$ for $D > \sqrt{2}$: in this case, for a fixed value of η, d_{14}, and θ, the capacity $\mathsf{C}_{4,\text{lower}}^{\text{bpsk}}$ as a function of d_{12} exhibits the same behavior of $\Delta\mathsf{C}_3$ (see Remark 7) and $\mathsf{C}_{4,\text{upper}}|_{M\gg 1}$ (see Remark 10).

[10]Let $f(X,Y) \triangleq X/Y$ be a transformation of the two random variables X and Y. Let $\mu_X \triangleq \mathbb{E}(X)$ and $\mu_Y \triangleq \mathbb{E}(Y)$, the first-order Taylor approximation for $\mathbb{E}[f(X,Y)]$ is given by $\mathbb{E}[f(X,Y)] = f(\mu_X,\mu_Y) + \mathbb{E}[f_x'(\mu_X,\mu_Y)\,(X-\mu_X)] + \mathbb{E}[f_y'(\mu_X,\mu_Y)\,(Y-\mu_Y)] = f(\mu_X,\mu_Y) = \mu_X/\mu_Y$, where $f_x'(\cdot)$ and $f_y'(\cdot)$ are the partial derivatives of the function $f(x,y)$ with respect to the real-valued variables x and y, respectively.

[11]Using similar bounding/approximation techniques, a lower bound on $\mathsf{C}_{4,\text{lower}}$ can be obtained for an arbitrary M-ary backscatter signal constellation, which however does not lend itself to easily interpretable results.

V. Numerical performance analysis

We present a Monte Carlo numerical analysis of the considered ambient backscatter network to validate and complete our theoretical analysis, with reference to both legacy and backscatter systems. All the ensemble averages (with respect to all the relevant fading channels and information-bearing symbols) and the outage probability of the legacy system are evaluated through 10^6 independent runs.

In all the experiments, we adopted the following simulation setting. We considered an indoor scenario by setting the reference distance $d_0 = 1$ m [36]. With reference to the Cartesian planes in Fig. 1, the nodes 1 (LTx) and 3 (LRx) have coordinates equal to $(-3,0)$ and $(3,0)$, respectively, i.e., $d_{13} = 6$ m. The position of the node 4 (BRx) depends on the network configuration: when the BRx and the LTx are co-located on the same device (see the left-side plot of Fig. 1), the coordinates of the LTRx are $(-3,0)$; on the other hand, when the BRx and the LTx are spatially-separated nodes (see the right-side plot of Fig. 1), the coordinates of the BRx are equal to $(-d_{13}/2 + d_{14}\,\cos(\phi-\theta), d_{14}\,\sin(\phi-\theta))$, with $d_{14} = 6$ m. In all the plots where the distance d_{12} varies, the node 2 (BTx) is placed along the line joining the nodes 1 and 2 (see Fig. 1). The multicarrier legacy system employs $M = 32$ subcarriers and a CP of length $L_{\text{cp}} = 8$. The legacy symbols are generated according to the corresponding capacity-achieving distribution $\mathbf{s} \sim \mathcal{CN}(\mathbf{0}_M, \sigma_s^2\,\mathbf{I}_M)$, with $\sigma_s^2 = 1$. On the other hand, the symbols transmitted by the backscatter device are equiprobably drawn from BPSK, 4-PSK (i.e., QPSK), and quaternary amplitude-shift keying (ASK) signal constellations. The order of the underlying discrete-time channels is set equal to $L_{13} = L_{12} = L_{23} = 3$, whereas the corresponding time offsets are fixed to $\theta_{13} = \theta_{12} = \theta_{23} = 1$, respectively. Moreover, unless otherwise specified, the path-loss exponent is chosen equal to $\eta = 2$. For the evaluation of the outage probability of the legacy system, we chose $R_s = 2$ b/s/Hz in (35).

A. Performance of the legacy system

Figs. 3 and 4 depict the ergodic capacity C_3 of the legacy system given by (22), in comparison with the ergodic capacity (24) when the backscatter system is in sleep mode (referred to as "w/o backscatter"), with $\text{SNR}_\text{L} = \sigma_s^2/\sigma_{v_3}^2 = 20$ dB, $\phi \in \{\pi/18, \pi/3\}$. In Fig. 3, the capacity values are reported as a function of the *mean square power wave reflection coefficient* $\mathbb{E}[|\Gamma(n)|^2] = \alpha^2\,\sigma_b^2$, with $d_{12} = 1.25$ m, whereas they are plotted against d_{12} in Fig. 4, with $\mathbb{E}[|\Gamma(n)|^2] = -20$ dB.

The capacity of the legacy system cannot degrade in the presence of the backscatter transmission (see Remark 5), in each operative condition. The gain $\Delta\mathsf{C}_3 = \mathsf{C}_3 - \mathsf{C}_3|_{\alpha=0}$

This article has been accepted for publication in a future issue of this journal, but has not been fully edited. Content may change prior to final publication. Citation information: DOI 10.1109/TCOMM.2017.2654448, IEEE Transactions on Communications

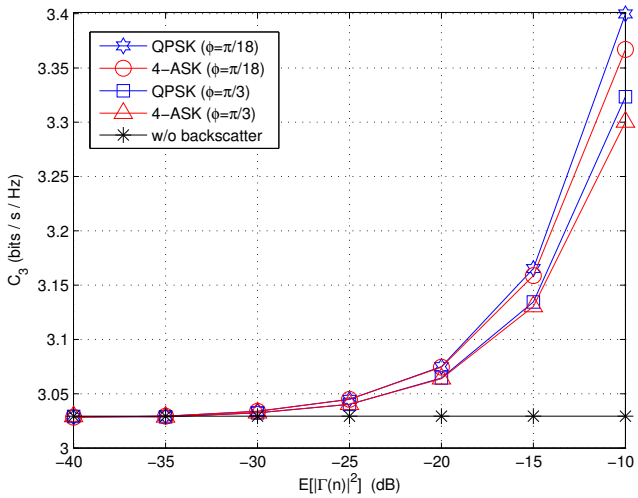

Figure 3. Ergodic capacity of the legacy system versus $\mathbb{E}[|\Gamma(n)|^2]$ for two backscatter signal constellations and two values of the angle ϕ.

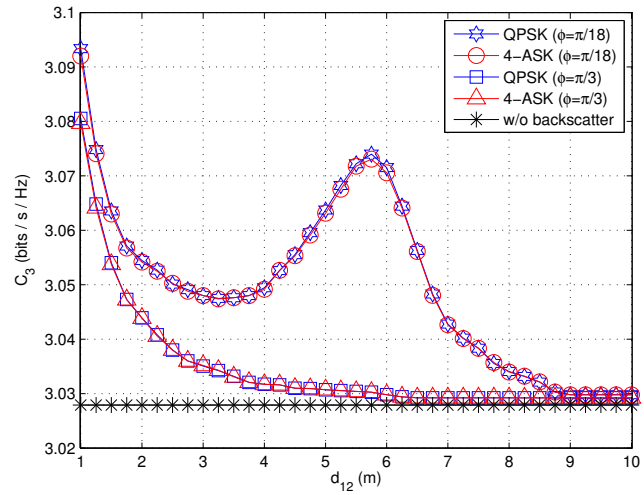

Figure 4. Ergodic capacity of the legacy system versus d_{12} for two backscatter signal constellations and two values of the angle ϕ.

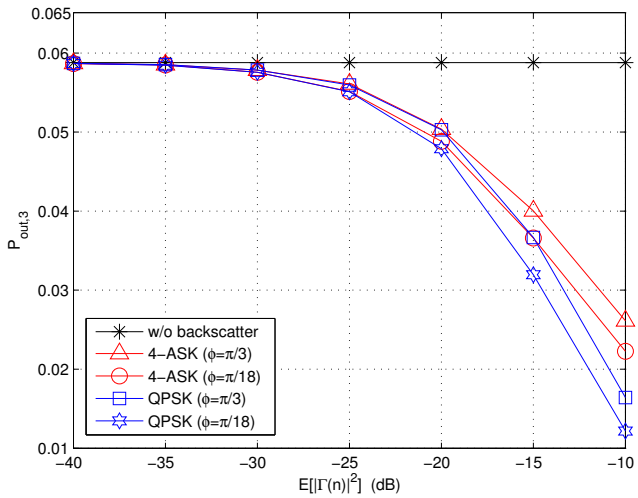

Figure 5. Outage probability of the legacy system versus $\mathbb{E}[|\Gamma(n)|^2]$ for two backscatter signal constellations and two values of the angle ϕ.

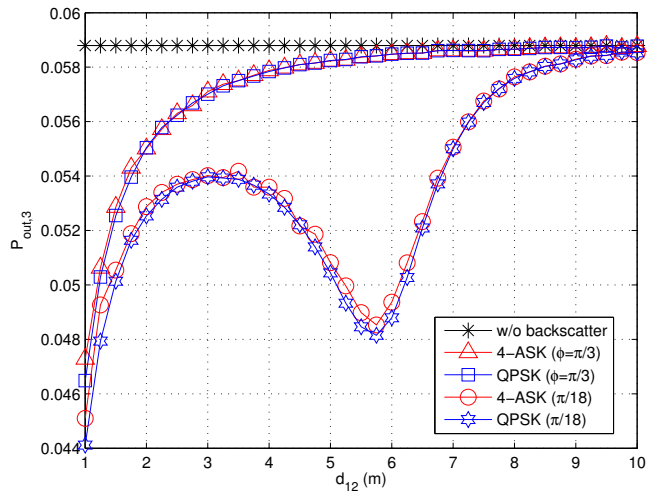

Figure 6. Outage probability of the legacy system versus d_{12} for two backscatter signal constellations and two values of the angle ϕ.

increases either when $\mathbb{E}[|\Gamma(n)|^2]$ is sufficiently large (see Remark 6) or the BTx is close to the LTx/LRx. It is also seen that, for a fixed Q, the choice of the backscatter signal constellation (ASK or PSK) does not lead to significantly different values of C_3. Moreover, results of Fig. 4 confirm the trends analytically predicted in Remark 7, by showing that C_3 monotonically decreases as the BTx moves away from the LTx when $\phi = \pi/3 \in \mathcal{A}$; on the other hand, when $\phi = \pi/18 \notin \mathcal{A}$, the capacity C_3 exhibits a local minimum at $d_{12}/d_{13} = d_{\text{min}}(\pi/18) = 0.5252 \implies d_{12} = 3.1512$ m and a local maximum at $d_{12}/d_{13} = d_{\text{max}}(\pi/18) = 0.9520 \implies d_{12} = 5.712$ and $d_{23} = 1.0603$ m (i.e., near the LRx). Similar conclusions can be drawn from the outage probability $\mathsf{P}_{\text{out},3}$ given by (35), as reported in Figs. 5 and 6. For completeness, Table I reports $\mathsf{C}_3|_{\alpha=0}$ and C_3 for three different values of the path-loss exponent η, when $\text{SNR}_{\text{L}} = 20$ dB, $\phi = \pi/18$, the backscatter modulation is QPSK, and $d_{12} = 1.25$ m.

We observe that even small values of $\Delta\mathsf{C}_3$ lead to noticeable increments in terms of data rate for the legacy transmission. For instance, it is seen from Fig. 3 that, when $\phi = \pi/18$ and the BTx employs a QPSK modulation, one gets $\Delta\mathsf{C}_3 = 0.0147$ b/s/Hz at $\mathbb{E}[|\Gamma(n)|^2] = -25$ dB. In this case, if the LTx is a Wi-Fi access point (AP) operating over a bandwidth of 20 MHz [5], [6], the gain is about 300 kbps.

B. Performance of the backscatter system when the LTx and BRx are co-located

We focus on the ergodic capacity C_1 of the backscatter system when the LTx and the BRx are co-located in the LTRx (see the left-side plot of Fig. 1), with $\mathbb{E}[|\Gamma(n)|^2] = -20$ dB. We report in Figs. 7 and 8 its upper bound $\mathsf{C}_{1,\text{upper}}$ given by (48) and lower bound $\mathsf{C}_{1,\text{lower}}$ given by (51) for PSK modulations, respectively, as a function of d_{12} for different values of $\text{SNR}_{\text{B},1}$. We also report in Fig. 8 the worst-case ergodic capacity of the backscatter system for the 4-ASK case obtained by numerically averaging (71) with respect to $\boldsymbol{\psi}$.

As predicted by the performance analysis developed in Subsection IV-A, both the upper and lower bounds are monotonically decreasing function of the distance between the LTRx and the BTx, for each value of $\text{SNR}_{\text{B},1}$. The slight performance

This article has been accepted for publication in a future issue of this journal, but has not been fully edited. Content may change prior to final publication. Citation information: DOI 10.1109/TCOMM.2017.2654448, IEEE Transactions on Communications

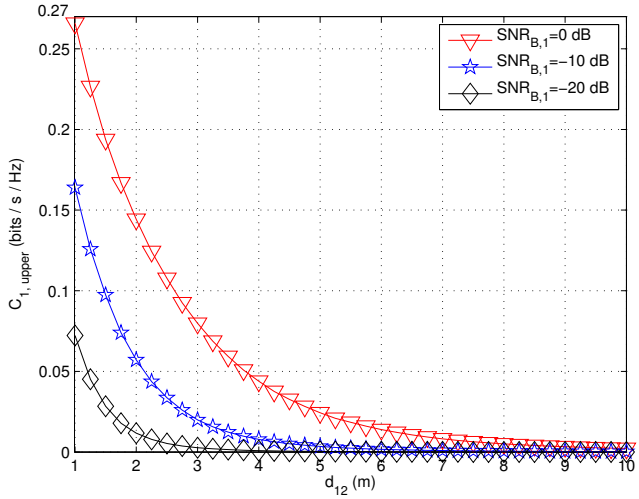

Figure 7. Best-case ergodic capacity of the backscatter system versus d_{12} for different values of $\text{SNR}_{\text{B},1}$ (LTx and BRx are co-located).

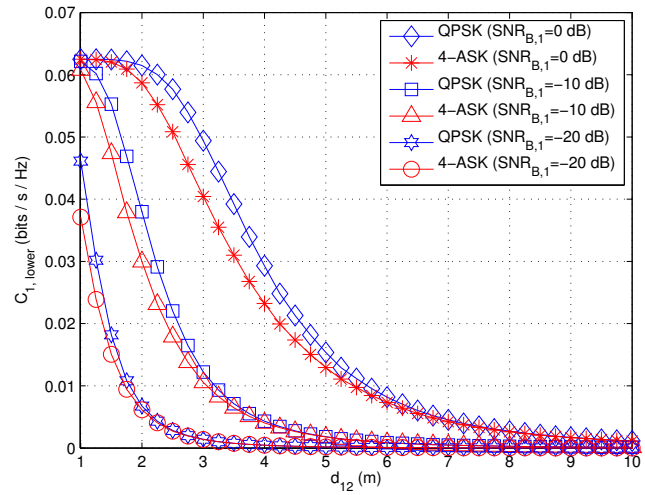

Figure 8. Worst-case ergodic capacity of the backscatter system versus d_{12} for different values of $\text{SNR}_{\text{B},1}$ and two backscatter signal constellations (LTx and BRx are co-located).

Table I
ERGODIC CAPACITIES FOR DIFFERENT VALUES OF η.

	$\eta=2$	$\eta=3$	$\eta=4$
$\mathsf{C}_3\|_{\alpha=0}$	3.0291	1.2700	0.3540
C_3	3.0748	1.3001	0.3658
$\mathsf{C}_{1,\text{upper}}$	0.2258	0.2060	0.1862
$\mathsf{C}_{1,\text{lower}}$	0.0625	0.0625	0.0624
$\mathsf{C}_{4,\text{upper}}$	0.1109	0.0488	0.0141
$\mathsf{C}_{4,\text{lower}}$	0.0220	0.0084	0.0012

advantage offered by the QPSK signal constellation over the 4-ASK one is due to the fact that the PSK modulation maximizes the cut-off rate in the case of equiprobable symbols (see Appendix A). Results not reported here show that the gap between $\mathsf{C}_{1,\text{upper}}$ and $\mathsf{C}_{1,\text{lower}}$ is reduced for increasing values of Q. The bounds $\mathsf{C}_{1,\text{upper}}$ and $\mathsf{C}_{1,\text{lower}}$ are reported in Table I for three different values of η, when $\text{SNR}_{\text{B},1}=0$ dB, the BTx employs a QPSK modulator, and $d_{12}=1.25$ m.

If the LTx is a Wi-Fi AP transmitting over a bandwidth of 20 MHz, which might be used to connect the BTx to the Internet [5], [6], we can infer from Fig. 8 that, when $\text{SNR}_{\text{B},1}=0$ dB, the backscatter communication can achieve at least 1 Mbps up to a range of $1-3$ m with a QPSK modulation, whereas a data rate of about 5 Mbps can be obtained in the best case over a range of $1-1.5$ m.

C. Performance of the backscatter system when the LTx and BRx are spatially-separated nodes

The last scenario under investigation is when the nodes LTx and BRx are spatially-separated nodes (see the right-side plot of Fig. 1), with $\theta\in\{\pi/18,\pi/3\}$ and $\mathbb{E}[|\Gamma(n)|^2]=-20$ dB.

Fig. 9 depicts the upper bound $\mathsf{C}_{4,\text{upper}}$ given by (60) as a function of d_{12} for different values of $\text{SNR}_{\text{B},4}$. Results corroborate the discussion reported in Remark 10, for each value of $\text{SNR}_{\text{B},4}$. In particular, if $\theta=\pi/3\in\mathcal{A}$, then $\mathsf{C}_{4,\text{upper}}$ monotonically decreases as the distance between the BTx and the LTx increases. When $\theta=\pi/18\notin\mathcal{A}$, the capacity $\mathsf{C}_{4,\text{upper}}$ assumes

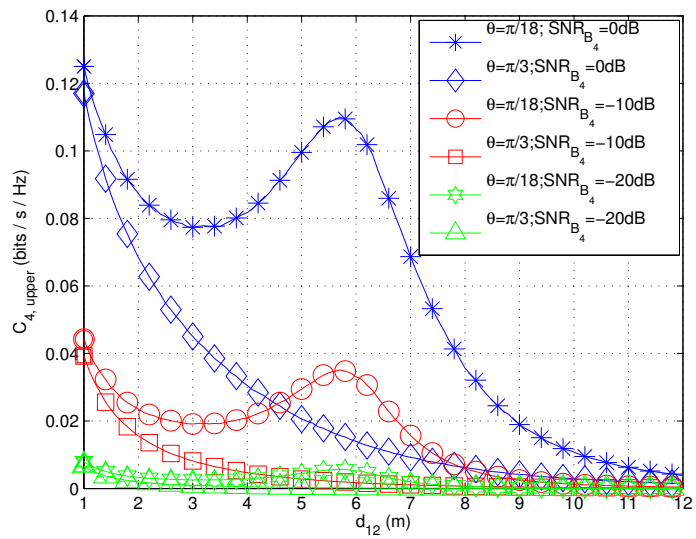

Figure 9. Best-case ergodic capacity of the backscatter system versus d_{12} for different values of $\text{SNR}_{\text{B},4}$ (LTx and BRx are spatially-separated nodes).

a global maximum when the BTx tends to be close to the LTx and a local maximum when the distance between the BTx and the BRx approaches d_0, i.e., $d_{12}/d_{14}=d_{\max}(\pi/18)=0.9520\implies d_{12}=5.712$ and $d_{24}=1.0603$, by taking on a local minimum when the BTx is about equidistant from the LTx and the BRx, i.e., $d_{12}/d_{14}=d_{\min}(\pi/18)=0.5252\implies d_{12}=3.1512$ and $d_{24}=2.9479$.

In Fig. 10, the capacity $\mathsf{C}_{4,\text{lower}}$ given by (63) is reported as a function of the $\text{SNR}_{\text{B},4}$ for different backscatter signal constellations, with $d_{12}=1.25$ m, whereas $\mathsf{C}_{4,\text{lower}}$ is reported in Fig. 11 as a function of d_{12}, with $\text{SNR}_{\text{B},4}=0$ dB. It is seen that, also in this case, PSK constellations ensure better performance in terms of cut-off rate when the symbols are equiprobable. Another interesting conclusion that can be drawn from Fig. 10 is that all curves exhibit a capacity saturation effect, for vanishingly small noise, which is due to the interference generated by the legacy system over the $1\to4$

This article has been accepted for publication in a future issue of this journal, but has not been fully edited. Content may change prior to final publication. Citation information: DOI 10.1109/TCOMM.2017.2654448, IEEE Transactions on Communications

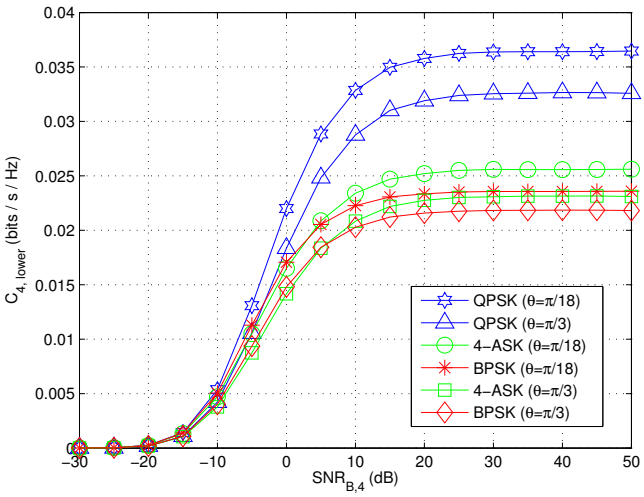

Figure 10. Worst-case ergodic capacity of the backscatter system versus $\mathrm{SNR}_{\mathrm{B},4}$ for three backscatter signal constellations and two values of the angle θ (LTx and BRx are spatially-separated nodes).

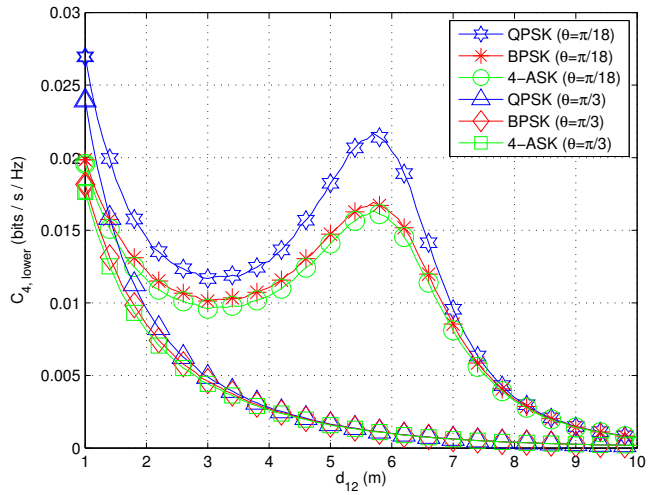

Figure 11. Worst-case ergodic capacity of the backscatter system versus d_{12} for three backscatter signal constellations and two values of the angle θ (LTx and BRx are spatially-separated nodes).

link. Moreover, independently of the considered backscatter signal constellation, the capacity $\mathsf{C}_{4,\mathrm{lower}}$ is a decreasing function of d_{12} when $\theta = \pi/3 \in \mathcal{A}$, whereas, for $\theta = \pi/18 \notin \mathcal{A}$, it exhibits a local minimum at $d_{12} = 3.1512$ and a local maximum at 5.712, which is in accordance with the discussion reported in Remark 12 with reference to the BPSK case. Table I reports the values of $\mathsf{C}_{4,\mathrm{upper}}$ and $\mathsf{C}_{4,\mathrm{lower}}$ for three different values of η, when $\mathrm{SNR}_{\mathrm{B},4} = 0$ dB, $\theta = \pi/18$, the backscatter modulation is QPSK, and $d_{12} = 1.25$ m.

When the LTx is a Wi-Fi AP transmitting over a bandwidth of 20 MHz, according to the results of Figs. 9 and 10, by employing a QPSK backscatter signal constellation, a data rate of about 2 Mbps can be achieved in the best case over a range of $1 - 1.5$ m at $\mathrm{SNR}_{\mathrm{B},4} = 0$ dB, whereas the worst-case achievable data rate is about $300 - 500$ kbps over a distance of 1.25 m at the same $\mathrm{SNR}_{\mathrm{B},4}$.

VI. Conclusions

We developed a framework for evaluating the ultimate achievable rates of a point-to-point network with ambient backscatter devices, by considering the influence of the backscatter transmission on the performance of the legacy system, from which energy is opportunistically harvested. Our theoretical results show that ambient backscatter allows a passive device to achieve satisfactory communication rates over short distances. As a by-product, the backscatter transmission can even ensure a performance improvement of the legacy system, provided that the latter one is designed to exploit the additional diversity arising from the backscatter process.

There are a number of open research issues. It should be investigated whether it is possible to develop tighter bounds for the backscatter system. Moreover, the achievable rate of a noncoherent backscatter system is still unknown. In this respect, it is of interest the practical design of ambient backscatter systems that can approach the predicted theoretical rates. Finally, results of our performance analysis pave the way towards various system-level optimizations. Among the others, an interesting issue is to analytically determine what is the optimal choice of $\mathbb{E}[|\Gamma(n)|^2]$ that ensures the best tradeoff between performance of legacy/backscatter systems and energy harvesting at the passive backscatter transmitter.

Appendix A
Proof of the Lower Bound (51)

By resorting to random coding arguments (see, e.g., [45]), it can be shown that the *cut-off rate*, which is defined as follows

$$R_1 \triangleq \max_{p_1,p_2,\ldots,p_Q} -\log \int \left[\sum_{q=1}^{Q} p_q \sqrt{f_{z_1\,|\,b=\beta_q,\boldsymbol{\psi}=\boldsymbol{\xi}}(x)}\right]^2 \mathrm{d}x \tag{70}$$

is a lower bound on $\mathsf{I}(b; z_1 \,|\, \boldsymbol{\psi} = \boldsymbol{\xi})$ at any SNR.

By using the properties of the logarithmic function, we observe that the objective function in (70) can be explicated as reported in (71) at the top of the next page, where the last but one equality is obtained by completion of the square in the exponent, whereas the last integral is 1 for any choice of the symbol set $\mathcal{B}$, since it is recognized as the integral of a univariate complex Gaussian pdf. Eq. (71) is valid for *any* finite-size symbol constellation, such as quadrature-amplitude modulation (QAM), PSK, orthogonal, lattice-type, or other. It is verified [45] that, for symbol constellations where the set of distances to other neighbors is invariant to the choice of the reference point, e.g., PSK and orthogonal modulations, the equiprobable assignment on the backscatter symbols (i.e., $p_q = 1/Q \ \forall q \in \mathcal{Q}$) maximizes (71). Therefore, remembering (41), (42), and (70), one yields (51).

Appendix B
Proof of the Upper Bound (60)

By using the chain rule for mutual information [31], [32], it can be proven that

$$\begin{aligned}\mathsf{I}(b; \mathbf{r}_4 \,|\, \boldsymbol{\Omega}_{124}, \boldsymbol{\Omega}_{14}, \mathbf{s}) &= \mathsf{I}(b; \mathbf{r}_4, \,|\, \boldsymbol{\Omega}_{124}, \boldsymbol{\Omega}_{14}) \\ &\quad + \mathsf{I}(b; \mathbf{s} \,|\, \mathbf{r}_4, \boldsymbol{\Omega}_{124}, \boldsymbol{\Omega}_{14}) \geq \mathsf{I}(b; \mathbf{r}_4, \,|\, \boldsymbol{\Omega}_{124}, \boldsymbol{\Omega}_{14})\end{aligned} \tag{72}$$

This article has been accepted for publication in a future issue of this journal, but has not been fully edited. Content may change prior to final publication. Citation information: DOI 10.1109/TCOMM.2017.2654448, IEEE Transactions on Communications

$$
\begin{aligned}
-\log \int \left[\sum_{q=1}^{Q} p_q \sqrt{f_{z_1\,|\,b=\beta_q,\boldsymbol{\psi}=\boldsymbol{\xi}}(x)}\right]^2 \mathrm{d}x &= -\log \sum_{q_1=1}^{Q}\sum_{q_2=1}^{Q} p_{q_1}\, p_{q_2} \int \frac{1}{\pi\sigma_{v_1}^2\,\|\boldsymbol{\xi}\|^2}\, e^{-\frac{\left|x-\alpha\,\|\boldsymbol{\xi}\|^2\,\beta_{q_1}\right|^2+\left|x-\alpha\,\|\boldsymbol{\xi}\|^2\,\beta_{q_2}\right|^2}{2\,\sigma_{v_1}^2\,\|\boldsymbol{\xi}\|^2}}\,\mathrm{d}x \\
&= -\log \sum_{q_1=1}^{Q}\sum_{q_2=1}^{Q} p_{q_1}\, p_{q_2}\, e^{-\frac{\alpha^2\,\|\boldsymbol{\xi}\|^2\,|\beta_{q_1}-\beta_{q_2}|^2}{4\,\sigma_{v_1}^2}} \int \frac{1}{\pi\sigma_{v_1}^2\,\|\boldsymbol{\xi}\|^2}\, e^{-\frac{\left|x-\alpha\,\|\boldsymbol{\xi}\|^2\,\frac{\beta_{q_1}+\beta_{q_2}}{2}\right|^2}{\sigma_{v_1}^2\,\|\boldsymbol{\xi}\|^2}}\,\mathrm{d}x \\
&= -\log \sum_{q_1=1}^{Q}\sum_{q_2=1}^{Q} p_{q_1}\, p_{q_2}\, e^{-\frac{\alpha^2\,\|\boldsymbol{\xi}\|^2\,|\beta_{q_1}-\beta_{q_2}|^2}{4\,\sigma_{v_1}^2}} \qquad (71)
\end{aligned}
$$

since $\mathsf{I}(b;\mathbf{r}_4,\,|\,\boldsymbol{\Omega}_{124},\boldsymbol{\Omega}_{14}) \geq 0$ by definition. Moreover, because subtracting a constant does not change mutual information [31], [32], one has (73) at the top of the next page, that is, since the BRx knows $\boldsymbol{\Omega}_{14}$ and $\mathbf{s}$, it can estimate b by subtracting $\mathbf{W}_{\text{IDFT}}\,\boldsymbol{\Omega}_{14}\,\mathbf{s}$ from (57), hence yielding $\hat{\mathbf{r}}_4 \triangleq \mathbf{r}_4 - \mathbf{W}_{\text{IDFT}}\,\boldsymbol{\Omega}_{14}\,\mathbf{s} = \alpha\,\mathbf{W}_{\text{IDFT}}\,\boldsymbol{\Omega}_{124}\,\mathbf{s}\,b + \mathbf{v}_4$. It follows that

$$
\begin{aligned}
&\mathsf{I}(b;\mathbf{r}_4 - \boldsymbol{\Omega}_{14}\,\mathbf{s}\,|\,\boldsymbol{\Omega}_{124}=\boldsymbol{\Xi}_{124},\boldsymbol{\Omega}_{14}=\boldsymbol{\Xi}_{14},\mathbf{s}=\mathbf{a}) \\
&\quad = \mathsf{h}(\hat{\mathbf{r}}_4\,|\,\boldsymbol{\Omega}_{124}=\boldsymbol{\Xi}_{124},\boldsymbol{\Omega}_{14}=\boldsymbol{\Xi}_{14},\mathbf{s}=\mathbf{a}) \\
&\quad\quad - \mathsf{h}(\hat{\mathbf{r}}_4\,|\,b,\boldsymbol{\Omega}_{124}=\boldsymbol{\Xi}_{124},\boldsymbol{\Omega}_{14}=\boldsymbol{\Xi}_{14},\mathbf{s}=\mathbf{a}) \qquad (74)
\end{aligned}
$$

where $\mathsf{h}(\hat{\mathbf{r}}_4\,|\,b,\boldsymbol{\Omega}_{124}=\boldsymbol{\Xi}_{124},\boldsymbol{\Omega}_{14}=\boldsymbol{\Xi}_{14},\mathbf{s}=\mathbf{a}) = \mathsf{h}(\mathbf{v}_4) = M\log(\pi e\,\sigma_{v_4}^2)$. As a consequence of the maximum-entropy theorem for complex random variables [42], one can obtain a further upper bound on (74) by using (75) at the top of the next page, with $\text{SNR}_{\text{B},4} \triangleq \alpha^2\sigma_b^2/\sigma_{v_4}^2$, where we have used the facts [15] that: (i) $\det(\mathbf{A}\,\mathbf{B}) = \det(\mathbf{A})\det(\mathbf{B})$ for arbitrary nonsingular matrices $\mathbf{A}\in\mathbb{C}^{n\times n}$ and $\mathbf{B}\in\mathbb{C}^{n\times n}$; (ii) $\det(\mathbf{W}_{\text{IDFT}})\det(\mathbf{W}_{\text{DFT}}) = 1$; (iii) for arbitrary vectors $\mathbf{x}\in\mathbb{C}^n$ and $\mathbf{y}\in\mathbb{C}^n$, $\det(\mathbf{I}_n + \mathbf{x}\,\mathbf{y}^{\text{H}}) = 1 + \mathbf{x}^{\text{H}}\mathbf{y}$. Henceforth, accounting for (72)–(75), the bound (60) follows from (58).

Appendix C
Proof of the lower bound (63)

As in Subsection IV-A, we rely on the fact that

$$
R_4 \leq \mathsf{I}(b;\mathbf{r}_4\,|\,\boldsymbol{\Omega}_{124}=\boldsymbol{\Xi}_{124},\boldsymbol{\Omega}_{14}=\boldsymbol{\Xi}_{14}) \qquad (76)
$$

where R_4 is the cut-off rate when the backscatter symbols are assumed to be equiprobable, that is,

$$
R_4 \triangleq -\log \int \left[\frac{1}{Q}\sum_{q=1}^{Q} \sqrt{f_{\mathbf{r}_4\,|\,b=\beta_q,\boldsymbol{\Omega}_{124}=\boldsymbol{\Xi}_{124},\boldsymbol{\Omega}_{14}=\boldsymbol{\Xi}_{14}}(\mathbf{x})}\right]^2 \mathrm{d}\mathbf{x}. \qquad (77)
$$

Eq. (57) shows that $\mathbf{r}_4\,|\,b = \beta_q,\boldsymbol{\Omega}_{124} = \boldsymbol{\Xi}_{124},\boldsymbol{\Omega}_{14} = \boldsymbol{\Xi}_{14} \sim \mathcal{CN}[\mathbf{0}_M,\mathbf{K}_4(\beta_q,\boldsymbol{\Xi}_{124},\boldsymbol{\Xi}_{14})]$, with $\mathbf{K}_4(\beta_q,\boldsymbol{\Xi}_{124},\boldsymbol{\Xi}_{14}) \triangleq \mathbb{E}(\mathbf{r}_4\,\mathbf{r}_4^{\text{H}}\,|\,b = \beta_q,\boldsymbol{\Omega}_{124} = \boldsymbol{\Xi}_{124},\boldsymbol{\Omega}_{14} = \boldsymbol{\Xi}_{14}) = \mathbf{W}_{\text{IDFT}}\,\mathbf{R}_4(\beta_q,\boldsymbol{\Xi}_{124},\boldsymbol{\Xi}_{14})\,\mathbf{W}_{\text{DFT}}$, where $\mathbf{R}_4(\beta_q,\boldsymbol{\Xi}_{124},\boldsymbol{\Xi}_{14}) \triangleq \alpha^2\,\sigma_s^2\,\boldsymbol{\Xi}_{124}\,\boldsymbol{\Xi}_{124}^*\,|\beta_q|^2 + \alpha\,\sigma_s^2\,\boldsymbol{\Xi}_{124}\,\boldsymbol{\Xi}_{14}^*\,\beta_q + \alpha\,\sigma_s^2\,\boldsymbol{\Xi}_{124}^*\,\boldsymbol{\Xi}_{14}\,\beta_q^* + \sigma_s^2\,\boldsymbol{\Xi}_{14}\,\boldsymbol{\Xi}_{14}^* + \sigma_{v_4}^2\,\mathbf{I}_M$ is a diagonal matrix. By using the properties of the determinant [15], we observe that R_4 can be explicated as reported in (78) at the top of this page, where we have omitted to explicitly indicate the dependence of $\mathbf{K}_4(\cdot)$ and $\mathbf{R}_4(\cdot)$ on $\boldsymbol{\Xi}_{124}$ and $\boldsymbol{\Xi}_{14}$, and the last integral is the hypervolume of a multivariate complex Gaussian pdf. By virtue of (59) and (76), one obtains (63).

References

[1] C. Boyer and S. Roy, "Backscatter communication and RFID: Coding, energy, and MIMO analysis", *IEEE Trans. Commun.*, vol. 62, pp. 770–785, Mar. 2014.

[2] D. Darsena, G. Gelli, and F. Verde, "Exploiting noncircularity in backscattering communications", in *Proc. of the 12th Int. Symp. Wireless Commun. Systems (ISWCS)*, Brussels, Belgium, Aug. 2015, pp. 1-5.

[3] O. Bello and S. Zeadally, "Intelligent device-to-device communication in the Internet of Things", *IEEE Syst. J.*, vol. 10, pp. 1172–1182, Sep. 2016.

[4] V. Liu, A. Parks, V. Talla, S. Gollakota, D. Wetherall, and J.R. Smith, "Ambient backscatter: Wireless communication out of thin air", in *Proc. of ACM SIGCOMM'13*, Hong Kong, China, Aug. 2013, pp. 39–50.

[5] B. Kellogg, A. Parks, S. Gollakota, J.R. Smith, and D. Wetherall, "Wi-Fi backscatter: Internet connectivity for RF-powered devices", in *Proc. of ACM SIGCOMM'14*, Chicago, Illinois, USA, Aug. 2014, pp. 607–618.

[6] D. Bharadia, K. Joshi, M. Kotaru, S. Katti, "BackFi: High throughput WiFi backscatter", in *Proc. of ACM SIGCOMM'15*, London, United Kingdom, Aug. 2015, pp. 283–296.

[7] Z. Ma, T. Zeng, G. Wang, and F. Gao, "Signal detection for ambient backscatter system with multiple receiving antennas", in *Proc. of IEEE 14th Canadian Workshop Inf. Theory (CWIT)*, St. John's, NL, Canada, July 2015, pp. 50-53.

[8] K. Lu, G. Wang, F. Qu, and Z. Zhong, "Signal detection and BER analysis for RF-powered devices utilizing ambient backscatter", in *Proc. of Int. Conf. Wireless Commun. & Signal Process. (WCSP)*, Nanjing, China, Oct. 2015, pp. 1-5.

[9] G. Wang, F. Gao, Z. Dou, and C. Tellambura, "Uplink detection and BER analysis for ambient backscatter communication systems", in *Proc. of IEEE Global Commun. Conf. (GLOBECOM)*, San Diego, CA, USA, Dec. 2015, pp. 1-6.

[10] H. Shariatmadari *et al.*, "Machine-type communications: Current status and future perspectives toward 5G systems", *IEEE Commun. Mag.*, vol. 53, pp. 10–17, Sep. 2015.

[11] S. Bi, C.K. Ho, and R. Zhang, "Wireless powered communication: Opportunities and challenges", *IEEE Commun. Mag.*, vol. 53, pp. 117–125, Apr. 2015.

[12] X. Lu *et al.*, "Wireless networks with RF energy harvesting: A contemporary survey", *IEEE Commun. Survey & Tutorials*, vol. 17, pp. 757–789, second quarter 2015.

[13] A. Sabharwal et al., "In-band full-duplex wireless: Challenges and opportunities," *IEEE J. Select. Areas Commun.*, vol. 32, pp. 1637–1652, Sep. 2014.

[14] D. Darsena, G. Gelli, and F. Verde, "Performance analysis of ambient backscattering for green Internet of Things", in *Proc. of IEEE Int. Symp. Personal, Indoor and Mobile Radio Commun. (PIMRC)*, Valencia, Spain, Sep. 2016, pp. 324–329.

[15] R. A. Horn and C. R. Johnson, *Matrix Analysis*, Cambridge: Cambridge University Press, 1990.

[16] Z. Wang and G.B. Giannakis, "Wireless multicarrier communications – where Fourier meets Shannon," *IEEE Signal Processing Mag.*, vol. 17, pp. 29–48, May 2000.

[17] S.R. Saunders, *Antennas and Propagation for Wireless Communication Systems*, New York: Wiley, 1999.

[18] D. Arnitz, U. Muehlmann, and K. Witrisal, "Wideband characterization of backscatter channels: Derivations and theoretical background", *IEEE Trans. Antennas Propag.*, vol. 60, pp. 257–266, Jan. 2012.

[19] H. Stockman,"Communication by means of reflected power", *Proc. IRE*, vol. 36, pp. 1196–1204, Oct. 1948.

This article has been accepted for publication in a future issue of this journal, but has not been fully edited. Content may change prior to final publication. Citation information: DOI 10.1109/TCOMM.2017.2654448, IEEE Transactions on Communications

$$\begin{aligned}\mathsf{I}(b;\mathbf{r}_4\,|\,\boldsymbol{\Omega}_{124},\boldsymbol{\Omega}_{14},\mathbf{s}) &= \mathsf{I}(b;\mathbf{r}_4-\mathbf{W}_{\text{IDFT}}\,\boldsymbol{\Omega}_{14}\,\mathbf{s}\,|\,\boldsymbol{\Omega}_{124},\boldsymbol{\Omega}_{14},\mathbf{s})\\ &= \mathbb{E}_{\boldsymbol{\Omega}_{124},\boldsymbol{\Omega}_{14},\mathbf{s}}\left[\mathsf{I}(b;\mathbf{r}_4-\mathbf{W}_{\text{IDFT}}\,\boldsymbol{\Omega}_{14}\,\mathbf{s}\,|\,\boldsymbol{\Omega}_{124}=\boldsymbol{\Xi}_{124},\boldsymbol{\Omega}_{14}=\boldsymbol{\Xi}_{14},\mathbf{s}=\mathbf{a})\right]\end{aligned} \tag{73}$$

$$\begin{aligned}\mathsf{h}(\hat{\mathbf{r}}_4\,|\,\boldsymbol{\Omega}_{124}=\boldsymbol{\Xi}_{124},\boldsymbol{\Omega}_{14}=\boldsymbol{\Xi}_{14},\mathbf{s}=\mathbf{a}) &\leq \log\left\{(\pi e)^M\det\left(\mathbb{E}\left[\hat{\mathbf{r}}_4\,\hat{\mathbf{r}}_4^{\mathrm{H}}\,|\,\boldsymbol{\Omega}_{124}=\boldsymbol{\Xi}_{124},\boldsymbol{\Omega}_{14}=\boldsymbol{\Xi}_{14},\mathbf{s}=\mathbf{a}\right]\right)\right\}\\ &= \log\left[(\pi e\,\sigma_{v_4}^2)^M\left(1+\text{SNR}_{\text{B},4}\,\|\boldsymbol{\Xi}_{124}\,\mathbf{a}\|^2\right)\right]\end{aligned} \tag{75}$$

$$\begin{aligned}R_4 &= -\log\sum_{q_1=1}^{Q}\sum_{q_2=1}^{Q}\frac{1}{Q^2}\int\frac{e^{-\frac{\mathbf{x}^{\mathrm{H}}\left[\mathbf{K}_4^{-1}(\beta_{q_1})+\mathbf{K}_4^{-1}(\beta_{q_2})\right]\mathbf{x}}{2}}}{\pi^M\sqrt{\det\left[\mathbf{K}_4(\beta_{q_1})\right]\det\left[\mathbf{K}_4(\beta_{q_2})\right]}}\,\mathrm{d}\mathbf{x}\\ &= -\log\sum_{q_1=1}^{Q}\sum_{q_2=1}^{Q}\frac{\det\left\{2\,\left[\mathbf{K}_4^{-1}(\beta_{q_1})+\mathbf{K}_4^{-1}(\beta_{q_2})\right]^{-1}\right\}}{Q^2\sqrt{\det\left[\mathbf{K}_4(\beta_{q_1})\right]\det\left[\mathbf{K}_4(\beta_{q_2})\right]}}\int\frac{e^{-\frac{\mathbf{x}^{\mathrm{H}}\left[\mathbf{K}_4^{-1}(\beta_{q_1})+\mathbf{K}_4^{-1}(\beta_{q_2})\right]\mathbf{x}}{2}}}{\pi^M\det\left\{2\,\left[\mathbf{K}_4^{-1}(\beta_{q_1})+\mathbf{K}_4^{-1}(\beta_{q_2})\right]^{-1}\right\}}\,\mathrm{d}\mathbf{x}\\ &= \log Q-\log\left[1+\frac{2^M}{Q}\sum_{q_1=1}^{Q}\sum_{\substack{q_2=1\\ q_2\neq q_1}}^{Q}\frac{1}{\sqrt{\det\left[\mathbf{R}_4(\beta_{q_1})\right]\det\left[\mathbf{R}_4(\beta_{q_2})\right]}\det[\mathbf{R}_4^{-1}(\beta_{q_1})+\mathbf{R}_4^{-1}(\beta_{q_2})]}\right]\end{aligned} \tag{78}$$

[20] S.J. Thomas, E. Wheeler, J. Teizer, and M.S. Reynolds, "Quadrature amplitude modulated backscatter in passive and semipassive UHF RFID systems", *IEEE Trans. Microw. Theory Tech.*, vol. 60, pp. 1175–1182, Apr. 2012.

[21] D.D. King,"The measurement and interpretation of antenna scattering", *Proc. IRE*, vol. 37, pp. 770–777, July 1949.

[22] K. Kurokawa, "Power waves and the scattering matrix", *IEEE Trans. Microw. Theory Tech.*, vol. 13, pp. 194–202, Mar. 1965.

[23] S. Thomas and M.S. Reynolds, "A 96 Mbit/sec, 15.5 pJ/bit 16-QAM modulator for UHF backscatter communication", in *Proc. of IEEE Int. Conf. RFID*, Orlando, Florida, USA, Apr. 2012, pp. 185–190.

[24] D. Arnitz, U. Muehlmann, and K. Witrisal, "Tag-based sensing and positioning in passive UHF RFID: Tag reflection", in *Proc. of 3rd Int. EURASIP Workshop RFID Technol.*, Cartagena, Spain, Sep. 2010, pp. 51–56.

[25] S. Thomas and M.S. Reynolds, "QAM backscatter for passive UHF RFID tags", in *Proc. of IEEE Int. Conf. RFID*, Orlando, Florida, USA, Apr. 2010, pp. 210–214.

[26] R.C. Hansen,"Relationships between antennas as scatterers and as radiators", *Proc. IEEE*, vol. 77, pp. 659–662, May 1989.

[27] U. Mengali and A.N. D'Andrea, *Synchronization Techniques for Digital Receivers*, New York: Plenum, 1997.

[28] M. Morelli, C.-C.J. Kuo, and M.-O. Pun, "Synchronization techniques for orthogonal frequency division multiple access (OFDMA): A tutorial review," *Proc. IEEE*, vol. 95, pp. 1394–1427, July 2007.

[29] B. Picinbono, "On circularity," *IEEE Trans. Signal Process.*, vol. 42, pp. 3473–3482, Dec. 1994.

[30] I.E. Telatar, "Capacity of multi-antenna Gaussian channels," *Eur. Trans. Telecommun.*, vol. 10, pp. 585–595, Nov./Dec. 1999.

[31] R.G. Gallager, *Information Theory and Reliable Communication*, New York: Wiley, 1968.

[32] T.M. Cover and J.A. Thomas, *Elements of Information Theory*, New York: Wiley, 1991.

[33] E. Biglieri, J.G. Proakis, and S. Shamai, "Fading channels: Information-theoretic and communications aspects," *IEEE Trans. Inf. Theory*, vol. 44, pp. 2916–2692, Oct. 1998.

[34] J.D. Griffin and G. Durgin, "Gains for RF tags using multiple antennas," *IEEE Trans. Antennas Propag.*, vol. 56, pp. 563–570, Feb. 2008.

[35] T. Betlehem and A.J. Coulson, "Distribution of the sum of a complex Gaussian and the product of two complex Gaussians", *Proc. of Australian Commun. Theory Workshop (AusCTW)*, Wellington, New Zealand, Jan.-Feb. 2012, pp. 126-129.

[36] T.S. Rappaport, *Wireless Communications: Principles and Practice (2nd Edition)*, Prentice Hall, Upper Saddle River, NJ, 2001.

[37] J.N. Laneman, D. Tse, and G.W. Wornell, "Cooperative diversity in wireless networks: efficient protocols and outage behavior," *IEEE Trans. Inf. Theory*, vol. 50, pp. 3062–3080, Sept. 2004.

[38] F. Verde and A. Scaglione, "Randomized space-time block coding for distributed amplify-and-forward cooperative relays", *Proc. of IEEE Int. Conf. Acoustics, Speech and Signal Process. (ICASSP)*, Dallas, Texas, Mar. 2010, pp. 3030-3033.

[39] L. Ozarow, S. Shamai, and A. Wyner, "Information theoretic considerations for cellular mobile radio," *IEEE Trans. Veh. Technol.*, vol. 43, pp. 359 – 378, May 1994.

[40] M. Morelli and U. Mengali, "A comparison of pilot-aided channel estimation methods for OFDM systems," *IEEE Trans. Signal Process.*, vol. 49, pp. 3065–3073, Dec. 2001.

[41] J G. Smith, "The information capacity of amplitude and variance-constrained scalar Gaussian channels," *Inf. Contr.*, vol. 18, pp. 203–219, 1971.

[42] F.D. Neeser and J.L. Massey, "Proper complex random processes with applications to information theory," *IEEE Trans. Inf. Theory*, vol. 39, pp. 1293–1302, July 1993.

[43] Y. Wu and S. Verdú, "The impact of constellation cardinality on Gaussian channel capacity," in *Proc. of the 48th Ann. Allerton Conf. Commun. Contr. and Comp. (Allerton)*, Allerton, IL, USA, Sep.-Oct. 2010, pp. 620–628.

[44] A. Papoulis. *Probability, Random variables, and Stochastics Processes (3rd ed.).* McGraw-Hill, Singapore, 1991.

[45] S.G. Wilson. *Digital Modulation and Coding.* Englewood Cliffs, NJ: Prentice Hall, 1996.

[46] T.L. Marzetta and B.M. Hochwald, "Capacity of a mobile multiple-antenna communication link in Rayleigh flat fading," *IEEE Trans. Inf. Theory*, vol. 45, pp. 139–157, Jan. 1999.

[47] B.M. Hochwald and T.L. Marzetta, "Unitary space-time modulation for multiple-antenna communications in Rayleigh flat fading," *IEEE Trans. Inf. Theory*, vol. 46, pp. 543–564, Mar. 2000.

[48] L. Zheng and D.N.C. Tse, "Communication on the Grassmann manifold:

A geometric approach to the noncoherent multiple-antenna channel," *IEEE Trans. Inf. Theory*, vol. 48, pp. 359–383, Feb. 2002.

Donatella Darsena (M'06-SM'16) received the Dr. Eng. degree *summa cum laude* in telecommunications engineering in 2001, and the Ph.D. degree in electronic and telecommunications engineering in 2005, both from the University of Napoli Federico II, Italy.

From 2001 to 2002, she was an engineer in the Telecommunications, Peripherals and Automotive Group, STMicroelectronics, Milano, Italy. Since 2005, she has been an Assistant Professor with the Department of Engineering, University of Napoli Parthenope, Italy. She has also held teaching positions at the University of Napoli Federico II, Italy. Her research activities lie in the area of statistical signal processing, digital communications, and communication systems. In particular, her current interests are focused on equalization, channel identification, narrowband-interference suppression for multicarrier systems, space-time processing for cooperative communications systems and cognitive communications systems, and software-defined networks.

Giacinto Gelli was born in Napoli, Italy, on July 29, 1964. He received the Dr. Eng. degree *summa cum laude* in electronic engineering in 1990, and the Ph.D. degree in computer science and electronic engineering in 1994, both from the University of Napoli Federico II.

From 1994 to 1998, he was an Assistant Professor with the Department of Information Engineering, Second University of Napoli. Since 1998 he has been with the Department of Electrical Engineering and Information Technology, University of Napoli Federico II, first as an Associate Professor, and since November 2006 as a Full Professor of Telecommunications. He also held teaching positions at the University Parthenope of Napoli.

His research interests are in the broad area of signal and array processing for communications, with current emphasis on multicarrier modulation systems and space-time techniques for cooperative and cognitive communications systems.

Francesco Verde (M'10-SM'14) was born in Santa Maria Capua Vetere, Italy, on June 12, 1974. He received the Dr. Eng. degree *summa cum laude* in electronic engineering from the Second University of Napoli, Italy, in 1998, and the Ph.D. degree in information engineering from the University of Napoli Federico II, in 2002. Since December 2002, he has been with the University of Napoli Federico II. He first served as an Assistant Professor of signal theory and mobile communications and, since December 2011, he has served as an Associate Professor of telecommunications with the Department of Electrical Engineering and Information Technology. His research activities include cyclostationarity-based techniques for blind identification, equalization and interference suppression for narrowband modulation systems, code-division multiple-access systems, multicarrier modulation systems, space-time processing for cooperative and cognitive communications systems, and software-defined networks. Prof. Verde has served as an Associate Editor for the IEEE SIGNAL PROCESSING LETTERS since November 2014. He was an Associate Editor of the IEEE TRANSACTIONS ON SIGNAL PROCESSING from September 2010 to October 2014 and a Guest Editor of the EURASIP JOURNAL ON ADVANCES IN SIGNAL PROCESSING in 2010.